Static crushing of wood based sandwich composite tubes

R. Guélou, Florent Eyma, Arthur Cantarel, Samuel Rivallant, Bruno Castanié

Static crushing of wood based sandwich composite tubes

R. Guélou[a], F. Eyma[a], A. Cantarel[a], S. Rivallant[a], B. Castanié[a,*]

[a]Institut Clément Ader (ICA), ISAE, CNRS UMR 5312-INSA-Mines Albi-UPS, Toulouse, France

* Corresponding author: bruno.castanie@insa-toulouse.fr

Keywords: Wood veneers, Poplar, Composites, Sandwich, Crushing, Energy absorption, Tube, Static,

Abstract This study presents static compression of sandwich tubes for crash applications in the transportation industry. The tubes were made from "I214" poplar veneers for the core, and carbon or glass woven plies reinforced with epoxy resin composites for the skins. The number of I214 layers in the core was varied between 2 and 6 while keeping the same number of plies for the skins. The results reveal interesting energy absorption performance of such structures in static, together with a coupling effect. In comparison with reference, all-carbon tubes, the sandwich tubes with carbon fibre skins having six I214 poplar plies showed an increase in mass of 75.2 g (+ 271%), a slightly degraded Specific Energy Absorption (- 7.2 J / g, - 10%), and an increase in the energy absorbed (+ 3,017 J, + 242%). For sandwich tubes with glass fibre skins having six I214 poplar plies, the SEA improved (+ 16 J / g, + 75%), the energy absorbed increased by 2,192 J (+ 602%) and the mass increased by 75.3 g (+ 314%). The SEA levels obtained were of the order of 61.2 J / g for sandwich tubes with carbon fibres and 32.5 J / g for those made of glass fibres (average values from static tests on all configurations).

1. Introduction

Wood is a material that traditionally has multiple applications: in the transport, naval, nuclear transport, furniture, and civil engineering domains or even in energy recovery (heating) from recycled products [1], [2], [3]. Wood also meets societal demands for a low-carbon society: rigorous management of resources, local supply and the use of healthy, renewable, ecological materials [4], [5]. In recent decades, it has experienced strong development in the construction of buildings. It is also an abundant,

local, economic, renewable resource with very low embodied energy [4,5]. The use of wood in means of transport had been forgotten, but it is in the process of being rediscovered. It was the main material in aviation until World War II [6], e.g. in the famous Mosquito (Fig. 1), nicknamed “the Wooden Wonder”. Its structure consisted of sandwich panels with skins formed from birch plies and a balsa core. It was manufactured in 7,781 units, with "one shot" half-fuselage manufacture, and could reach 612 km/h. In the automotive sector, only the English manufacturer Morgan offered cars with an ash superstructure, which nevertheless had an aluminium chassis. At Le Mans in 1967, the Costin-Nathan (Fig. 1) had an aeronautical plywood frame, with doors made of fibreglass, and weighed only 410 kg [7].

Fig. 1. The mosquito and its manufacture in two half fuselages, and the Costin-Nathan with a wooden frame, 1100 cm3, 410 kg.

Today, studies have identified wood as one of the credible substitute materials to meet the objectives of a bio-economy [8] and some directly question the possibility of its use in the automobile [9,10]. In particular, an Austrian programme on the subject was launched in 2016 [11]. There is now renewed interest in searching for lightweight construction solutions using wood—in particular in the form of plywood or sandwich with various shaped cores from classic okoume and poplar plywood core sandwich [12] to a lattice wood core made from PLA and olive wood dust [13] to a corrugated radiata pine plywood core sandwich [14] to a beech wood prismatic core with veneer sheets as skins [15] or a three grid sandwich made of spruce and a core made of jute fibres [16]. The current regulatory safety constraints [17] require the crash behaviour of vehicles to satisfy certain criteria (Head Injury Criterion, etc.). Recent studies have shown that wood, alone or in combination with current composites, behaves very well under low energy and low velocity impacts [18], [19], [20] and, in particular, in compression after impact [21], [22], [23], [24]. There are very few studies on wood crash behaviour. However, poplar, in the form of massive test pieces, has shown very good results [25] and the authors have recently

demonstrated that tubes made of poplar plies have an SEA that is roughly 1/3 that of carbon tubes, but for a layer cost that is divided by 40 [26].

In the field of crashworthiness, their low density and their high specific resistances enable composite materials to provide very interesting specific energy absorption when the failure mode is adequate [29]. They can serve as a model for understanding the ruin modes of wood-based sandwich tubes. Three failure modes predominate in crushing: local buckling, splaying, and fragmentation. These failure modes were presented in [26] and defined by Farley and Hull [28], [29]. The energy absorption potential of a material is generally evaluated using the SEA. Composite materials can exceed metallic materials in terms of SEA thanks to their low density [30]. SEA is dependent on multiple parameters, such as geometric shape [31], position, and the number and orientation of composite layers [29], [32]. The use of sandwich-type structures has also grown in the construction of composite parts. The aim of combining a core and skins is generally to obtain a light structure, with high flexural rigidity and good thermal insulation characteristics [6], [33].

In crash-type applications, the core tends to increase the level of energy absorbed like with foam filler [34], [35], [36], hybrid tubes aluminium/CFRP [37] or honeycomb-filler [38], [39]. Depending on the rise in energy level and core weight, a gain in SEA is often observed. Wood is also used as core material, but rarely for crash applications. Two studies of triggers have been carried out [40], [41] on solid balsa associated with glass or carbon fibre skins, and made it possible to obtain stable crushing, improving the SEA of the composite sandwich panels. The use of redwood and pine chips [42] or sawdust [43] by inserting them as core materials allowed an increase in absorbed energy. Reddy [44] filled rectangular tubes in mild steel with tropical wood. He showed that the length of the folds of the tubes was reduced by the presence of such a core: if the length was reduced, there were more bulges and therefore more energy was necessary for their formation.

Although wood has been little studied as a core material for crash applications, it has, nevertheless, demonstrated its ability to absorb energy during crashes [26], and the question of crushing it as a core

material in the form of plywood piqued our interest. This article analyses the static crushing of sandwich tubes having a winding of I214 poplar veneers as a core, associated with skins of carbon or glass fibres.

2. Materials, test tubes and set-up description

2.1. Materials and manufacturing

Each wood/composite or composite alone sandwich tube was always made up of 4 composite layers: a sandwich tube had 2 interior layers and 2 exterior layers of composites; a single composite tube therefore had a total of 4 layers. The sandwich tubes were defined as follows: [2CFRP- [0n] -2CFRP] describing 2 carbon fabric layers inside, n poplar veneers oriented at 0° (0° being the longitudinal axis of the tube), and 2 carbon fabric layers outside. The composite tubes were then defined as follows: [CFRP] or [GFRP] depending on the nature of the fibres (Carbon or Glass). The orientation of the fabrics, balanced 2-2 twill, was always [0/90] to achieve a hoop effect due to the 90° fibres [29, 32]. The composite layers were made with carbon (M79 / 42% / 200T2 / CHR-3K, Hexcel) and glass (M9.6GF / 42% / 200T2 / G, Hexcel) pre-impregnated 2- 2 twill. These two prepregs had a basis weight of 345 g/m^2, inducing a theoretical fibre volume fraction of 44% and 39% for the carbon and the glass, respectively. The curing cycle for carbon was 20 min at 90 °C then 2h 20 min at 120 °C, and that of glass was 20 min at 90 °C then 1h at 120 °C. The core was stacked with 1 mm thick I214 poplar (Populus x euramericana cultivar I-214) veneers supplied by Garnica. Veneers density is 0.368 g/cm^3, and veneers are glued together between 8.8% and 9.8%HR.

The manufacturing of the sandwich tubes started with the stacking of the internal skins (carbon or glass) on a metal mandrel. Then, the pre-glued poplar veneers were wound (Fig. 2 (c) and (e)). The glue used to bond the veneers was Kleiberit PUR 510 Fiberbond, a one-component polyurethane-based adhesive which hardens by reaction with humidity, with a basis weight of 250 g/m^2. A curing step was then performed using heat-shrinkable bands wound around the entire specimen, which provided pressure during crosslinking. Secondly, the outer skins in carbon or glass fibres were stacked, followed by a final curing step using heat-shrink bands (Fig. 2 (d)). The tubes were then cut on each side and a chamfer at

45° was milled at one end over their entire thickness. Finally they were cut again to their final length of 120 mm (Fig. 2 (a) and (b)). The chamfer's role was to control the initiation side of the ruin and also to attenuate the peak load [45]. The specimens had an internal diameter of 50 mm and a density ranging from 647 to 851 kg/m3 for the carbon sandwich tubes and 656 to 855 kg/m3 for the glass ones. The density varied because it depended on the number of wood plies. (As the number of wood plies increased, the density decreased).

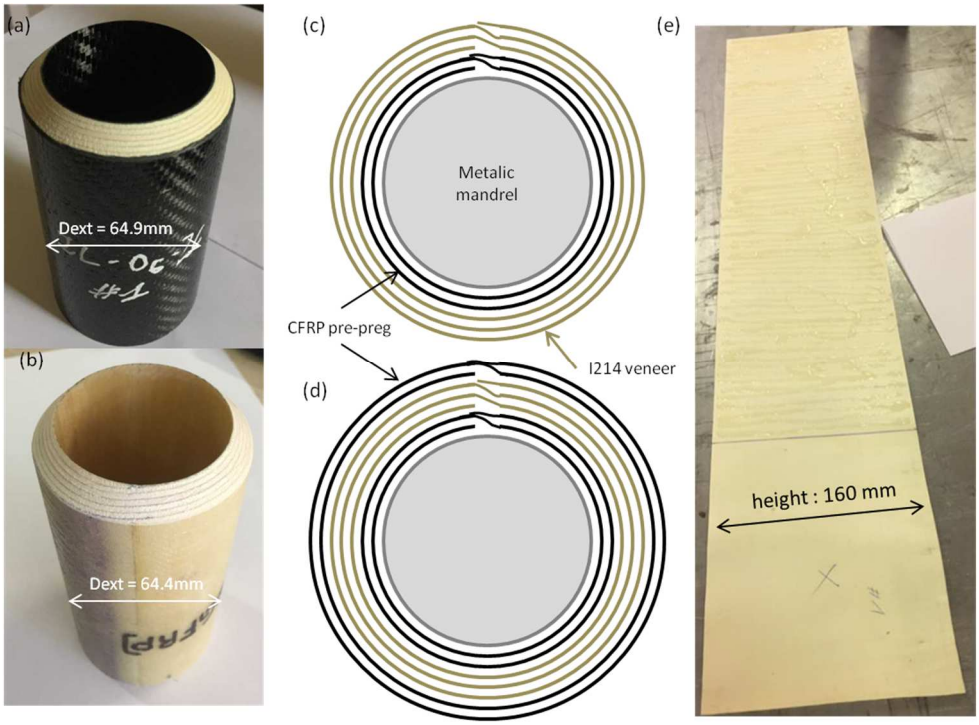

Fig. 2. Pristine tubes (a) [2CFRP-[0_6]-2CFRP]-#1, (b) [2GFRP-[0_6]-2GFRP]-#1, (c) First step in manufacturing, (d) Second step, (e) Pre-gluing of a I214 veneer strip before winding

For each configuration, three tubes were crushed in order to assess the repeatability of the results (Tab. 1).

	number of samples
[2CFRP-[90/0$_4$/90]-2CFRP]	3
[90/0$_4$/90] (already crushed in [26])	3
[2CFRP-[0$_6$]-2CFRP]	3
[2CFRP-[0$_5$]-2CFRP]	3
[2CFRP-[0$_4$]-2CFRP]	3
[2CFRP-[0$_3$]-2CFRP]	3
[2CFRP-[0$_2$]-2CFRP]	3
[CFRP]	3

	number of samples
[2GFRP-[0$_6$]-2GFRP]	3
[2GFRP-[0$_5$]-2GFRP]	3
[2GFRP-[0$_4$]-2GFRP]	3
[2GFRP-[0$_3$]-2GFRP]	3
[2GFRP-[0$_2$]-2GFRP]	3
[GFRP]	4
Total number of tubes	43

Tab.1. Summary of all configurations.

Static tensile tests (2 mm/min) were made from two veneers plies bonded together with the same glue and basis weight used for sandwich tubes manufacturing. A vacuum bag was used for curing 6 specimens (Fig. 3) at 120°C during 20 min. Results are presented in Tab. 2.

	Longitudinal			Transversal	
	E (MPa)	σ_{UTS} (MPa)	σ_{UCS} (MPa)	E (MPa)	σ_{UTS} (MPa)
Average	10 924	69	36 [47]	391	4.91
Standard deviation	893	14	/	41	0.74

Tab. 2. Static tensile tests results from two I214 plies glued and ultimate compression strength of I214 [47]

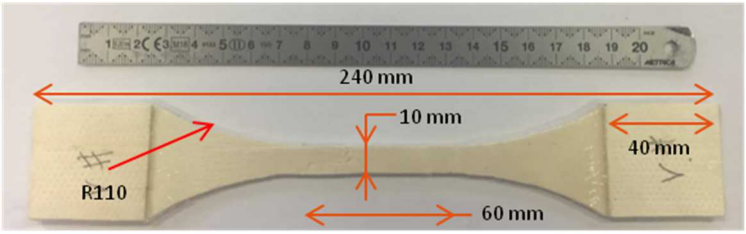

Fig. 3. Tensile specimen geometry inspired from [46] (inspired from NF-EN 408)

2.2. Static set-up and test analysis

During a stable crushing event, three phases were generally observed (Fig. 4). The first corresponded to a quasi-linear response in the force-displacement curve until the peak load was reached. This slope corresponded to the combination of two mechanisms: crushing and damage of the chamfer, and the linear compression of the pristine part of the tube. From the peak, the failure mode changed and followed a transition phase and then a plateau phase. Static crushes were performed on an MTS System traction machine equipped with a 100 kN load cell. The tests were interrupted after ¾ of the initial length of the tubes, i.e. 90 mm, had been crushed, and were carried out at a speed of 5 mm/min.

The criteria extracted from the tests were the following:

- F_{max}, corresponding to the maximum force recorded during the compression (N),
- $F_{plateau}$, defining the average force at the level of the plateau phase (N),
- CFE (Crush Force Efficiency), the ratio ($F_{plateau}/F_{max}$). It should be as close as possible to 1 to limit the forces in the rest of the structure [48],
- EA_{tot_80mm}, the energy (J) absorbed from the start of crushing up to 80 mm crushed,
- SEA_{tot_80mm}, representing the Specific Energy Absorption, also defined on the first 80 millimetres crushed and therefore calculated as follows: $\mathrm{SEA_{tot\_80mm}} = \frac{\mathrm{EA_{tot\_80mm}}}{\rho \times S \times d_{crushed}} = \frac{\mathrm{EA_{tot\_80mm}}}{M_{80mm}}$ (J/g), with ρ the average density of the tube (prepreg + glue + veneers), S the cross section, $d_{crushed}$ the crushed distance (here 80 mm), and M_{80mm} the mass of the 80 mm of crushed tube.

The SEA was calculated on the first 80 millimetres of each tube in order to be able to compare the absorbed energies, as the samples were not all crushed to exactly the same length (between 85 and 90 mm), especially during dynamic tests (not shown here).

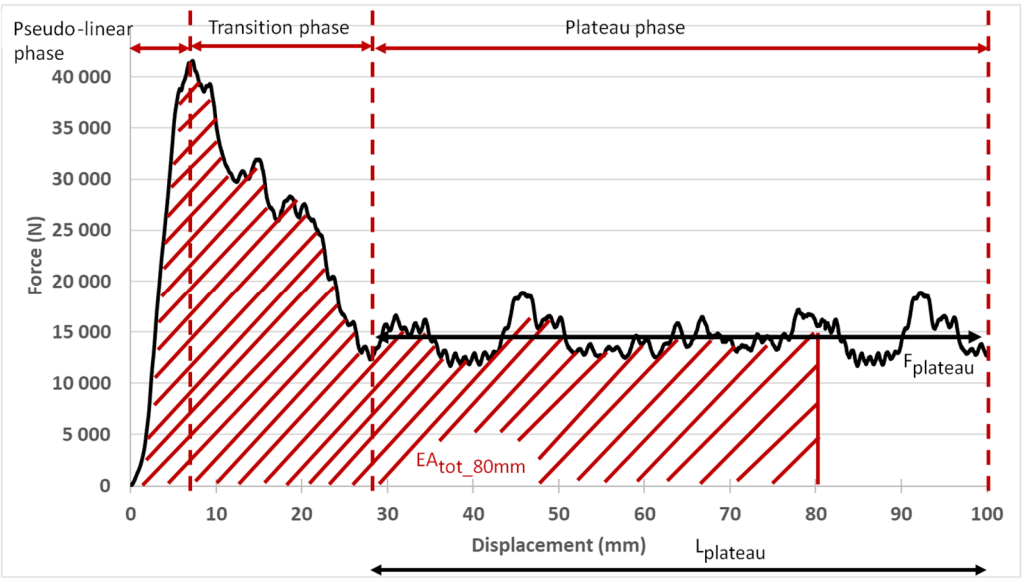

Fig. 4. Computation of EA_{tot_80mm}

3. Results and discussion

3.1. Core stacking influence

From previous work [28], the best configuration in terms of SEA was taken first to make the core: [90/0_4/90]. The objective of this part was to study the influence of the orientation of the plies in the core with this first stacking or with all layers oriented at 0°. The idea was to see if the "hoop effect" was better with the presence of inner and outer carbon woven carbon plies only or with the orientation of additional 90° layers of poplar. So the two following configurations were studied: [2CFRP- [90/0_4/90] -2CFRP] and [2CFRP- [0_6] -2CFRP]. In the latter, all the veneers in the core were oriented along the longitudinal axis of the tubes. Three tubes of each configuration were crushed statically at 5 mm/min (Fig. 5).

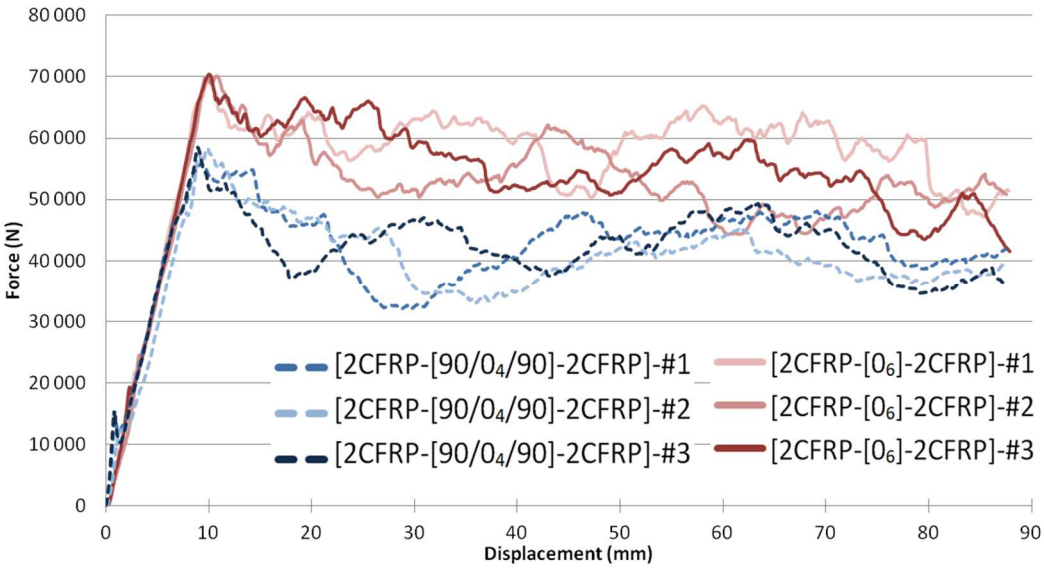

Fig. 5. Static force-displacement curves - influence of orientation of veneers in the core.

With regard to the force-displacement curves, the three phases mentioned in the literature review for the crushing of a tube were found. The pseudo-linear slope is slightly higher in favour in the configuration [2CFRP- [0_6] -2CFRP] for a stiffness with an average value of 7,5 N/mm, and an average value of 6,2 N/mm for the configuration [2CFRP- [90/0_4/90] -2CFRP]. The repeatability of the tests was quite good, with energy absorbed standard deviations of 101 and 241 J compared to average values of 3,248 and 4,264 J ([2CFRP- [90/0_4/90] -2CFRP] and [2CFRP- [0_6] -2CFRP] respectively).

	Mass g	Thickness mm	F_{max} N	$L_{plateau}$ mm	$F_{plateau}$ N	CFE	EA_{tot_80mm} J	SEA_{tot_80mm} J/g
[2CFRP-[90/0_4/90]-2CFRP] - #1	103.0	7.66	55 972	69.6	42 184	0.75	3 314	46.1
[2CFRP-[90/0_4/90]-2CFRP] - #2	102.0	7.72	58 426	68.9	39 682	0.68	3 132	43.9
[2CFRP-[90/0_4/90]-2CFRP] - #3	104.6	7.63	58 473	69.6	42 117	0.72	3 299	45.1
Average	**103.2**	**7.67**	**57 624**	**69.4**	**41 328**	**0.72**	**3 248**	**45.0**
Standard deviation	**1.3**	**0.05**	**1 430**	**0.4**	**1 426**	**0.04**	**101**	**1.1**
[2CFRP-[0_6]-2CFRP] - #1	102.4	7.44	69 646	75.5	59 051	0.85	4 503	63.0
[2CFRP-[0_6]-2CFRP] - #2	104.7	7.55	70 138	71.7	52 535	0.75	4 021	55.1

[2CFRP-[0_6]-2CFRP] - #3	101.7	7.38	70 439	73.0	55 067	0.78	4 267	60.5
Average	**102.9**	**7.46**	**70 074**	**73.4**	**55 551**	**0.79**	**4 264**	**59.5**
Standard deviation	**1.3**	**0.05**	**401**	**1.9**	**3 285**	**0.05**	**241**	**4.0**

Tab. 3. Static test results for [2CFRP-[90/0_4/90]-2CFRP] and [2CFRP-[0_6]-2CFRP]

In terms of performance, the sandwich tubes [2CFRP- [0_6] -2CFRP] proved to be superior to the configuration [2CFRP- [90/0_4/90] -2CFRP] both in terms of average crushing force (+14 220 N, or 34%), of absorbed energy (+1,016 J, or 31%) and in SEA (+ 14.5 J / g, or 32%) (Tab. 3). The performance difference can be explained by the difference of failure modes. It can also be explained by the fact that replacing the two poplar plies of the core oriented at 90° by plies at 0° provided a higher crush resistance. The 2-2 carbon twill is thus sufficient to ensure the "hoop effect" and stabilize the inner polar layers oriented at 0°. Concerning the failure modes, for the configuration [90/0_4/90], local buckling predominated, leading to a succession of folds accompanied by local splaying with the appearance of one or two petals (Fig. 6).

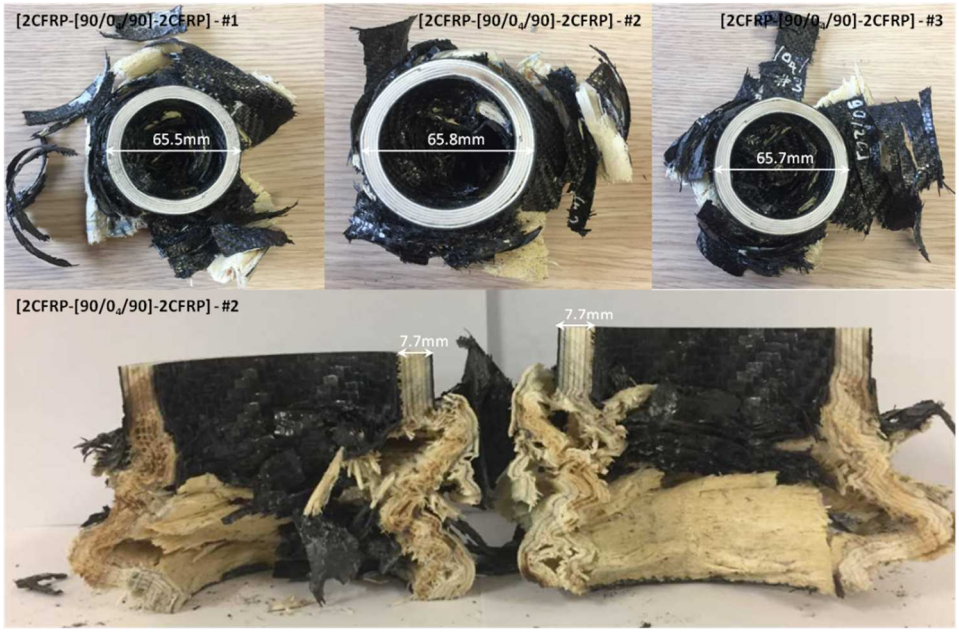

Fig. 6. Post mortem patterns of [2CFRP-[90/0_4/90]-2CFRP], tube #2 after cutting.

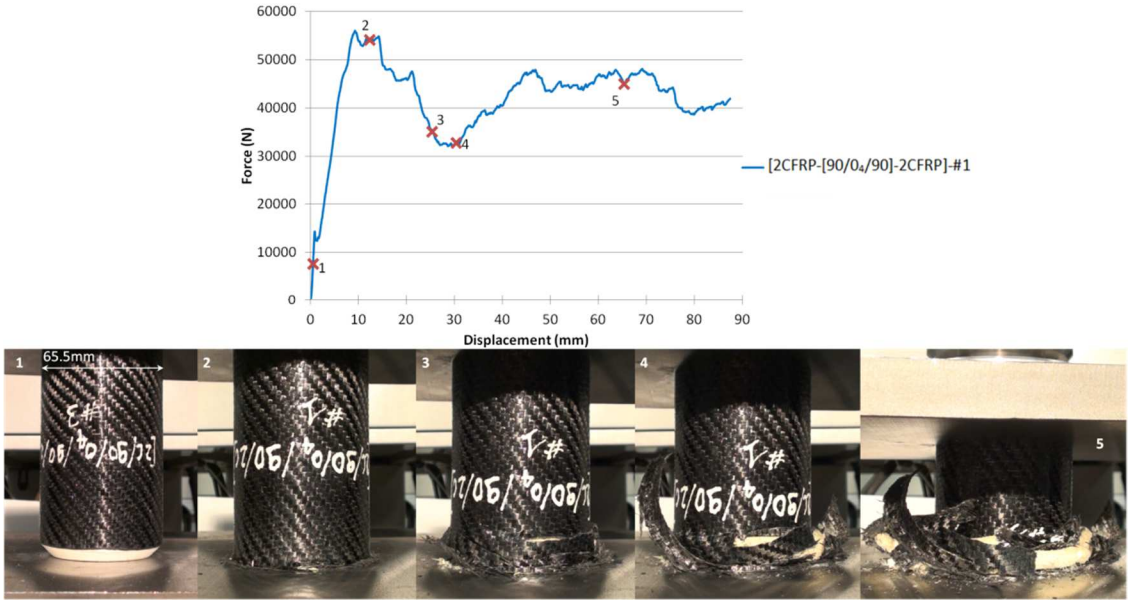

Fig. 7. Failure scenario for [2CFRP-[90/0_4/90]-2CFRP]- tube #1. Association between pictures and points on the force-displacement curve.

When loading began, the chamfer became damaged and flattened out (Fig. 7). As the crush progressed, the entire chamfer was damaged and the two outer plies of carbon participated in the crush. They then started to splay in and out of the tube (point 2 Fig. 7). The creation of folds in the core then began but, due to the carbon skins, the folds remained invisible during the crushing. When a fold is created, it probably imposes a large deformation on the carbon, leading to decohesion between the carbon and the wood and failure of the carbon over a few centimetres, creating carbon strips (point 3 Fig. 7).

The core configuration [0_6] mostly underwent splaying, which divided the thickness into two bundles. However, a whole part of the thickness was observed to bend without dividing into two separate bundles. The division of the thickness into two parts is probably conditioned by the creation of debris upstream (Fig. 8 tube # 1 after cutting). Very localized buckling could also appear, generating very few folds (Fig. 8 tube # 2 after cutting).

Fig. 8. Failure pattern of tubes [2CFRP-[0$_6$]-2CFRP] and tubes #1 and #2 after cutting.

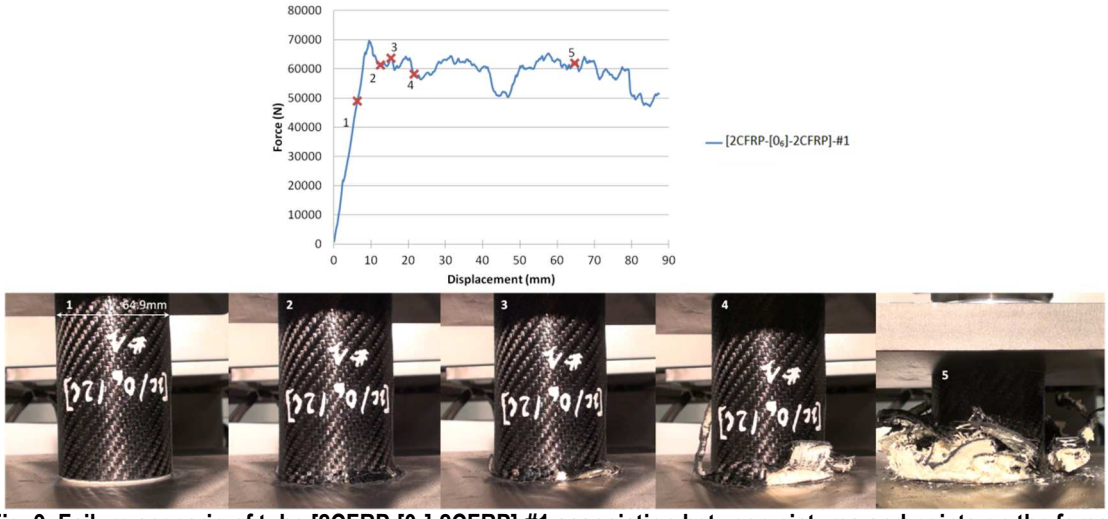

Fig. 9. Failure scenario of tube [2CFRP-[0$_6$]-2CFRP]-#1 association between pictures and points on the force-displacement curve

Once the chamfer was completely crushed and the two outer carbon plies started to be loaded, the carbon plies splayed into and out of the tube. As the composite skins splayed, the strains increased significantly and caused the fibres to break at 90°, thus generating the petals. As the crushing continued, the petals created continued to splay (Fig. 9).

In conclusion, the comparison of these two configurations shows that it is not necessary to orient I214 veneers at 90° in the core, as the "hoop effect" is provided by the carbon woven layer. It even appears that orienting the 6 veneers at 0° makes it possible to obtain higher energy levels at the same number of folds, and therefore at iso-mass and iso-cost.

3.2. Crushing with carbon skins

A study of the influence of the number of I214 poplar layers in the core was therefore carried out with only 0° folds. To do this, the following configurations were crushed: [2CFRP-[0_n]-2CFRP]$_{2\leq n\leq 6}$. Three specimens were tested for each configuration. All the static curves are shown in Fig. 10.

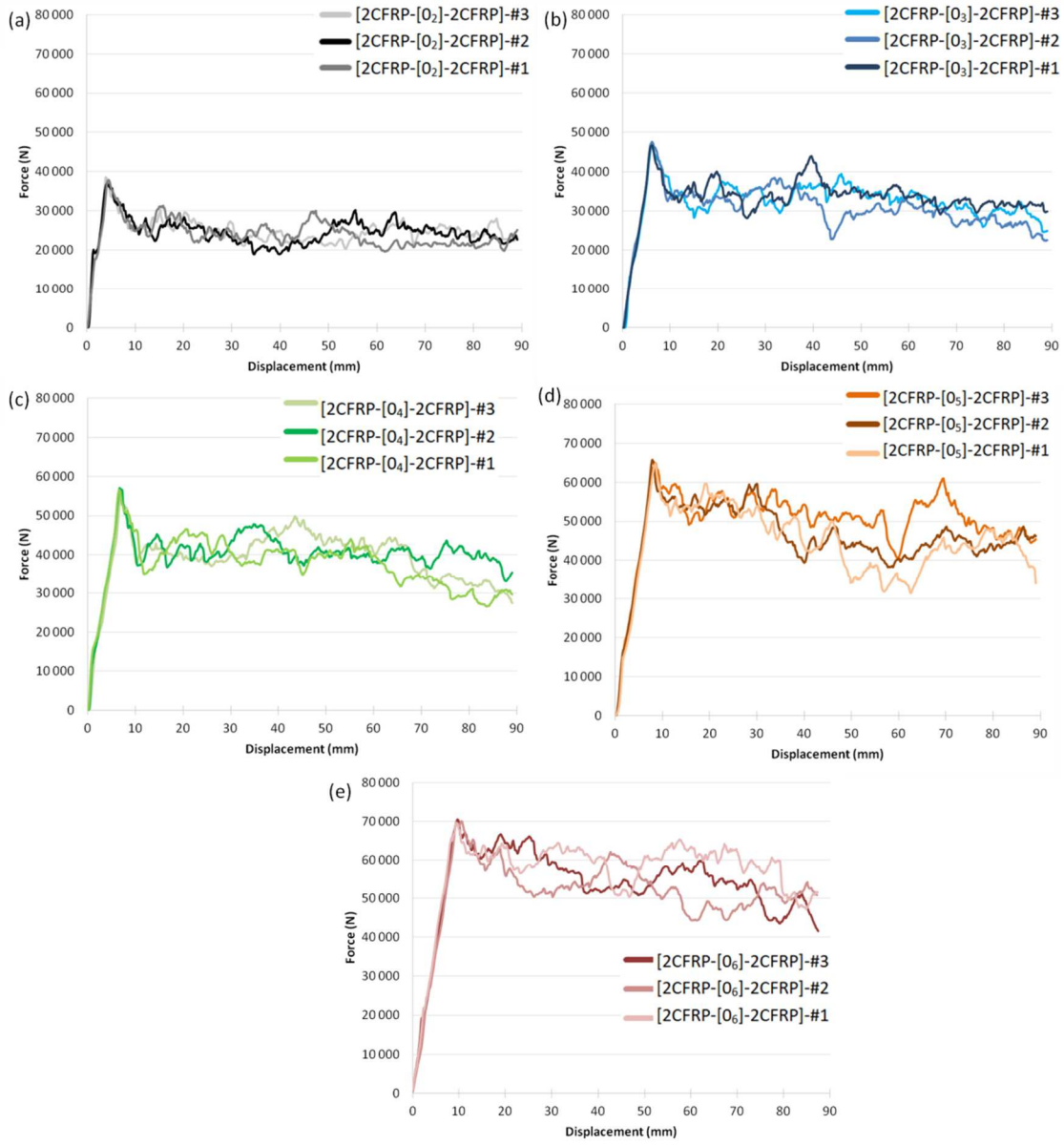

Fig. 10. Static force-displacement curves (a) [2CFRP-[0_2]-2CFRP], (b) [2CFRP-[0_3]-2CFRP], (c) [2CFRP-[0_4]-2CFRP], (d) [2CFRP-[0_5]-2CFRP], (e) [2CFRP-[0_6]-2CFRP]

Again, the three phases (initiation, transition and plateau) were found. Logically, the average value of the plateau effort rose as the number of poplar layers increased (Tab. 4).

	Mass	Thickness	F_{max}	$L_{plateau}$	$F_{plateau}$	CFE	EA_{tot_80mm}	SEA_{tot_80mm}
	g	mm	N	mm	N		J	J/g
[2CFRP-[0_2]-2CFRP] - #1	49.2	3.06	37 753	77.4	23 667	0.63	1 931	58.1
[2CFRP-[0_2]-2CFRP] - #2	48.8	2.98	36 931	77.8	24 111	0.65	1 965	59.6
[2CFRP-[0_2]-2CFRP] - #3	49.1	2.98	38 536	78.6	24 522	0,64	1 981	59.8
Average	**49.0**	**3.01**	**37 740**	**77.9**	**24 100**	**0.64**	**1 959**	**59.2**
Standard deviation	**0.2**	**0.05**	**803**	**0.6**	**428**	**0.01**	**26**	**0.9**
[2CFRP-[0_3]-2CFRP] - #1	61.8	3.99	46 703	77.1	33 804	0.72	2 679	64.1
[2CFRP-[0_3]-2CFRP] - #2	61.7	3.99	47 576	79.6	30 614	0.64	2 487	59.7
[2CFRP-[0_3]-2CFRP] - #3	61.3	4.01	47 168	78.4	32 760	0.69	2 623	63.2
Average	**61.6**	**4.00**	**47 149**	**78.3**	**32 393**	**0.69**	**2 596**	**62.3**
Standard deviation	**0.3**	**0.01**	**437**	**1.2**	**1 626**	**0.04**	**99**	**2.3**
[2CFRP-[0_4]-2CFRP] - #1	78.2	5.10	56 701	76.9	37 543	0.66	3 070	60.1
[2CFRP-[0_4]-2CFRP] - #2	73.7	5.03	57 088	78.5	40 721	0.71	3 226	64.5
[2CFRP-[0_4]-2CFRP] - #3	76.1	5.05	54 680	78.6	39 774	0.73	3 190	61.8
Average	**76.0**	**5.06**	**56 156**	**78.0**	**39 346**	**0.70**	**3 162**	**62.1**
Standard deviation	**2.2**	**0.04**	**1 293**	**0.9**	**1 632**	**0.03**	**81**	**2.2**
[2CFRP-[0_5]-2CFRP] - #1	87.7	6.28	64 694	77.4	45 211	0.70	3 555	58.8
[2CFRP-[0_5]-2CFRP] - #2	87.7	6.15	65 721	77.9	47 023	0.72	3 696	61.5
[2CFRP-[0_5]-2CFRP] - #3	89.5	6.17	64 929	79.2	51 892	0.80	4 059	66.1
Average	**88.3**	**6.20**	**65 115**	**78.2**	**48 042**	**0.74**	**3 770**	**62.2**
Standard deviation	**1.0**	**0.07**	**538**	**0.9**	**3 455**	**0.05**	**260**	**3.7**
[2CFRP-[0_6]-2CFRP] - #1	102.4	7.44	69 646	75.5	59 051	0.85	4 503	63.0
[2CFRP-[0_6]-2CFRP] - #2	104.7	7.45	70 138	71.7	52 535	0.75	4 021	55.1
[2CFRP-[0_6]-2CFRP] - #3	101.7	7.38	70 439	73.0	55 067	0.78	4 267	60.5
Average	**102.9**	**7.46**	**70 074**	**73.4**	**55 551**	**0.79**	**4 264**	**59.5**
Standard deviation	**1.6**	**0.04**	**401**	**19**	**3 285**	**0.05**	**241**	**4.0**

Tab. 4. Static test results [2CFRP-[0_n]-2CFRP]$_{2\leq n\leq 6}$

Regarding the failure mode of this configuration, as in the previous configurations, the failure was initiated via the flattening of the chamfer. With the chamfer flattened, the outer carbon skins came into contact with the compression plate and were forced to splay outward. Then, the 90° oriented carbon fibres of the 2-2 twill ply broke, creating petals in the tube as the crushing progressed (Fig. 11).

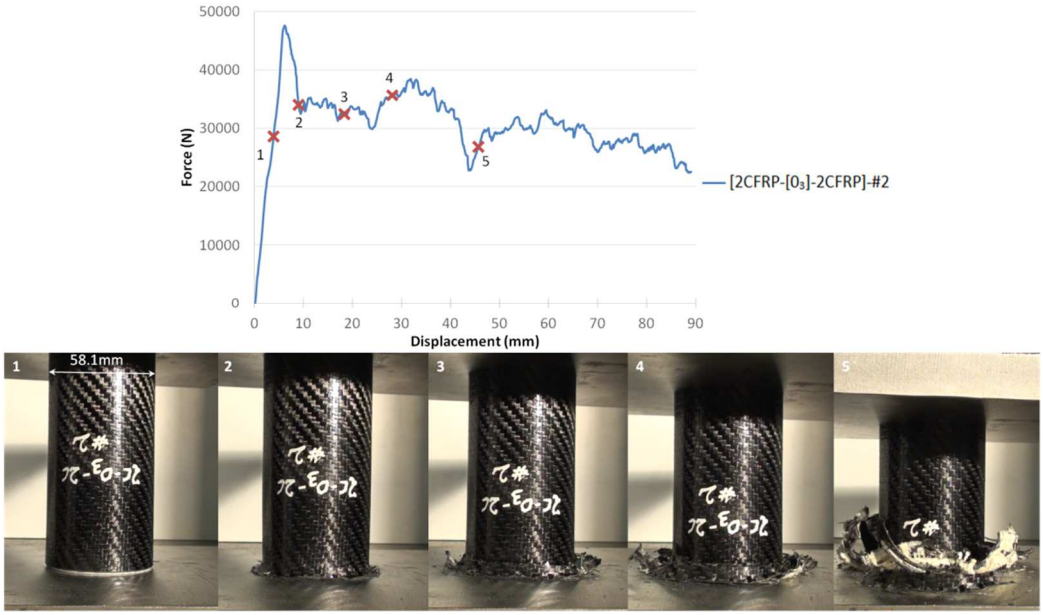

Fig. 11. Static failure of tube [2CFRP-[0$_3$]-2CFRP]-#2 association between pictures and points on the force-displacement curve

Thanks to the post-mortem observation and the cutting into two half tubes (Fig. 12), it could be observed that local buckling was present but not generalized, the predominant failure mode being splaying. The creation of debris probably conditioned the splaying. However, it can be observed in Fig. 12 (tube [2CFRP-[0$_4$]-2CFRP]-#1 after cutting) that part of the thickness did not separate into two beams but bent completely.

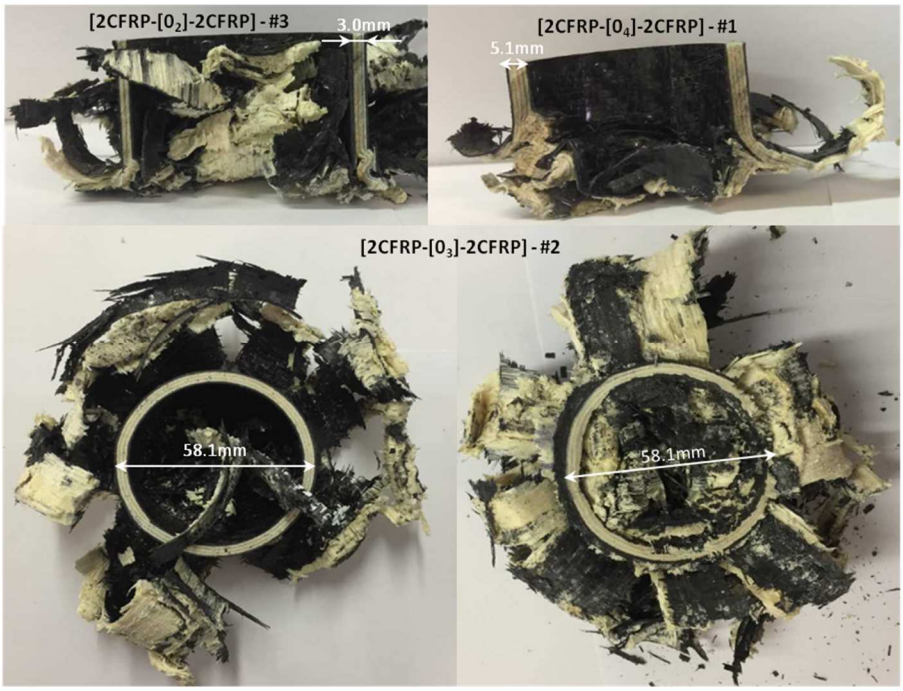

Fig. 12. Static failure of tube [2CFRP-[0$_3$]-2CFRP]-#2 and ½ tubes [2CFRP-[0$_2$]-2CFRP]-#3 and [2CFRP-[0$_4$]-2CFRP]-#1

The evolution of absorbed energy and SEA is plotted vs the number of I214 folds in Fig. 13 (a). The energy absorbed can be seen to increase linearly with the number of I214 folds. A linear regression gives: $EA_{tot\_80mm} = 576 \times nbre\ layers_{I214} + 851$. The directing coefficient, 576 J, represents the contribution of a single I214 ply oriented at 0° and 851 J can be considered as the contribution of the 4 carbon plies. The SEA_{tot_80mm} is almost constant, depending on the number of I214 folds, and oscillates around an average value of 61.1 J/g.

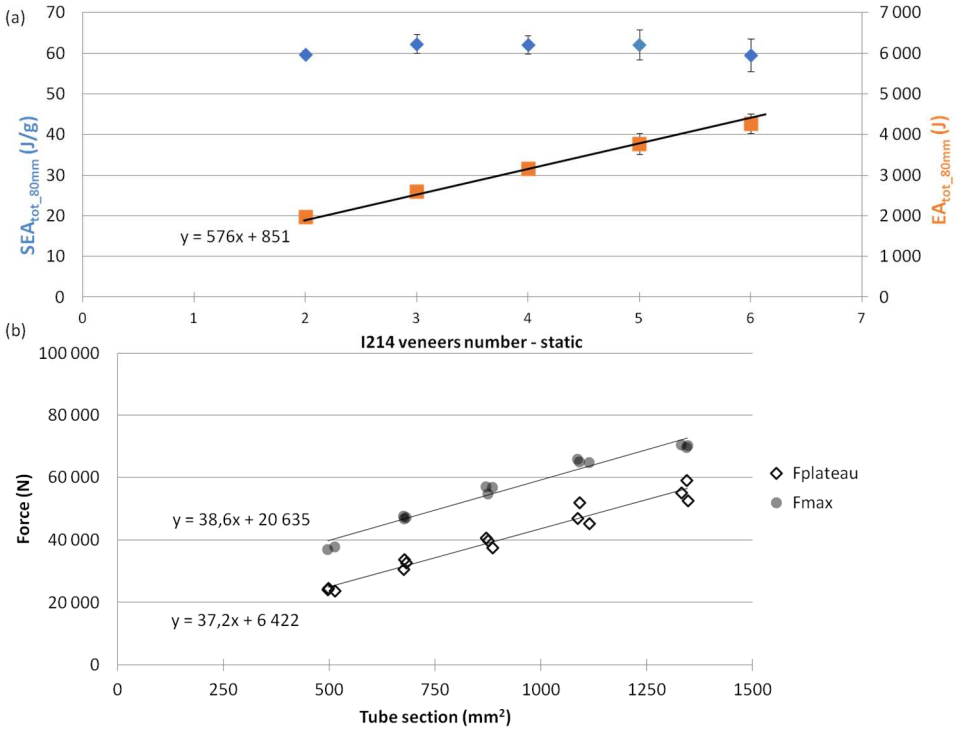

Fig. 13. Evolution of (a) EA_{tot_80mm} and (b) SEA_{tot_80mm} according to the number of I214 layers. Evolution of the peak force and the average force of the plateau versus the cross-section of the tubes with carbon fibre skins.

To understand the evolution of dissipated energies, it is interesting to represent the evolution of the peak force and the plateau average versus the cross-section of the tubes (Fig. 13 (b)). First, the peak load naturally increases with the number of poplar layers. However, the CFE is not degraded (Tab. 4) since the crushing plateau also increases. The average value of the CFE increases with the number of layers and approaches 1. The fact that the load peaks are higher than the average force of the plateau reflects a change in the failure mechanism between the initiation phase and the plateau: we do not observe splaying during initiation, although it is the main mode of failure during the plateau phase.

On the other hand, the failure mechanisms observed are similar from one core configuration to another, whether for the initiation phase or for the plateau. Moreover, the sections of the carbon folds are always the same. Therefore, the directing coefficient of the regression curves of Fig. 13 (b) can be interpreted as the mean value of the crushing stress of the core material I214 in the failure mode associated with each phase: 38.6 MPa at peak load, slightly greater than the 37.2 MPa obtained during the plateau. It should be noted that this stress is not an intrinsic parameter of the poplar material I214, unlike what can be calculated for some composite materials based on carbon fibres (T700/M21) which fail under localized fragmentation [49]. Here, it corresponds to the average stress induced by the overall failure mechanisms in the core and includes splaying and local buckling.

Finally, the y-intercept of the regression line for the peak load (20,635 N) shows that carbon fibre skins are much more efficient during the initiation phase than in the plateau phase (6,422 N). This can be explained by the failure mode of the skins, which tends to be fragmentation during the initiation, while it is splaying during the rest of the crushing. Furthermore, the standard deviation increases with the number of I214 folds (Tab. 4 and Fig. 13). This finding can be explained by the great variability of the properties of poplar as a material, especially in veneers.

3.3. Crushing with glass skins

The work done with the carbon fibre-epoxy resin skins was reproduced with the glass fibre-epoxy resin skins (same prepreg and 2-2 twill weave, but with a lower fibre volume fraction of 39%). The number of I214 layers studied was the same. The static test results are shown in Fig. 14.

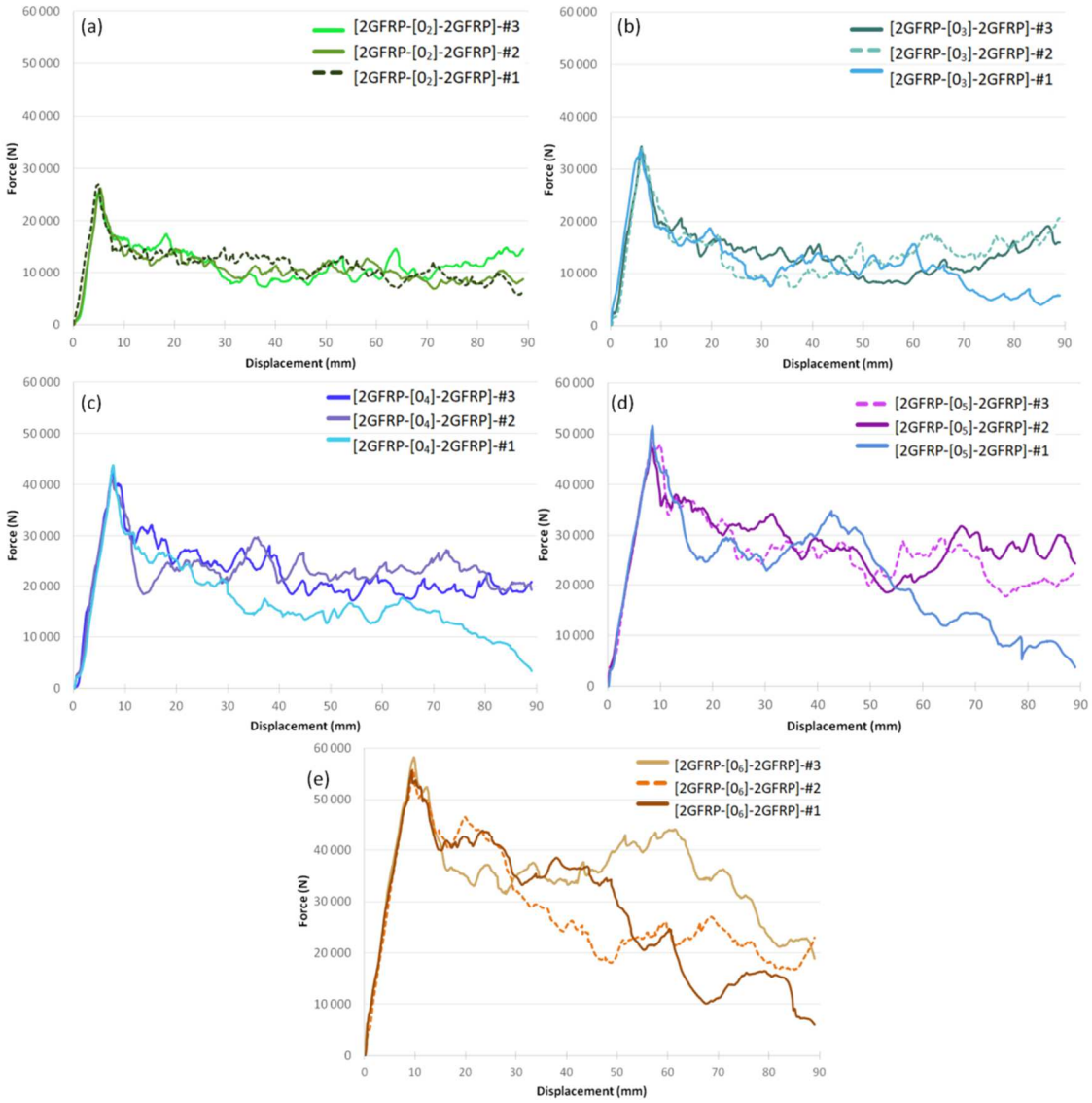

Fig. 14. Static force-displacement curves for tubes (a) [2GFRP-[0$_2$]-2GFRP], (b) [2GFRP-[0$_3$]-2GFRP], (c) [2GFRP-[0$_4$]-2GFRP], (d) [2GFRP-[0$_5$]-2GFRP], and (e) [2GFRP-[0$_6$]-2GFRP]

As with carbon sandwich tubes, a peak load is found, followed by a transition phase and then a plateau. The value of the plateau also increases with the number of I214 layers. The results of static crushing are presented in Tab. 5.

	Mass	Thickness	F_{max}	$L_{plateau}$	$F_{plateau}$	CFE	EA_{tot_80mm}	SEA_{tot_80mm}
	g	mm	N	mm	N	/	J	J/g
[2GFRP-[0_2]-2GFRP] - #1	46.3	2.84	26 941	81.2	11 061	0.41	952	30.3
[2GFRP-[0_2]-2GFRP] - #2	47.2	2.95	26 257	78.9	10 507	0.40	897	27.9
[2GFRP-[0_2]-2GFRP] - #3	47.2	2.82	25 312	80.7	11 443	0.45	919	28.7
Average	**46.8**	**2.87**	**26 170**	**80.3**	**11 004**	**0.42**	**923**	**29.0**
Standard deviation	**0.5**	**0.07**	**818**	**1.2**	**471**	**0.03**	**28**	**1.2**
[2GFRP-[0_3]-2GFRP] - #1	60.4	3.88	33 503	79.8	10 916	0.33	1 017	24.8
[2GFRP-[0_3]-2GFRP] - #2	58.8	3.83	34 029	76.4	13 386	0.39	1 108	27.8
[2GFRP-[0_3]-2GFRP] - #3	60.4	3.98	34 385	79.5	13 324	0.39	1 096	26.8
Average	**59.9**	**3.90**	**33 972**	**78.6**	**12 542**	**0.37**	**1 074**	**26.5**
Standard deviation	**0.9**	**0.08**	**444**	**1.9**	**1 409**	**0.04**	**49**	**1.5**
[2GFRP-[0_4]-2GFRP] - #1	72.8	4.95	43 829	77.3	15 941	0.36	1 444	29.1
[2GFRP-[0_4]-2GFRP] - #2	71.8	5.00	41 099	75.3	23 052	0.56	1 893	38.7
[2GFRP-[0_4]-2GFRP] - #3	72.2	4.84	43 396	77.3	22 031	0.51	1 824	37.0
Average	**72.3**	**4.93**	**42 775**	**76.6**	**20 341**	**0.48**	**1 720**	**34.9**
Standard deviation	**0.5**	**0.08**	**1 467**	**1.2**	**3 845**	**0.10**	**241**	**5.1**
[2GFRP-[0_5]-2GFRP] - #1	87.9	6.10	51 567	71.9	27 225	0.53	1 891	31.4
[2GFRP-[0_5]-2GFRP] - #2	88.5	6.16	47 267	78.7	28 264	0.60	2 259	37.2
[2GFRP-[0_5]-2GFRP] - #3	87.1	6.15	50 172	77.5	25 834	0.51	2 160	36.2
Average	**87.8**	**6.14**	**49 669**	**76.0**	**27 108**	**0.55**	**2 103**	**34.9**
Standard deviation	**0.7**	**0.03**	**2 194**	**3.6**	**1 220**	**0.04**	**191**	**3.1**
[2GFRP-[0_6]-2GFRP] - #1	99.7	7.27	55 551	74.3	26 396	0.48	2 397	34.9
[2GFRP-[0_6]-2GFRP] - #2	99.2	7.20	55 902	72.0	26 265	0.47	2 354	34.4
[2GFRP-[0_6]-2GFRP] - #3	98.9	7.19	58 206	72.4	34 325	0.59	2 917	42.8
Average	**99.3**	**7.22**	**56 553**	**72.9**	**28 995**	**0.51**	**2 556**	**37.4**
Standard deviation	**0.4**	**0.04**	**1 442**	**1.2**	**4 616**	**0.07**	**313**	**4.7**

Tab. 5. Results for static tests [2GFRP-[0_n]-2GFRP]$_{2\leq n\leq 6}$

The sandwich tubes with two or three I214 plies (Fig. 14 (a) and (b)) exhibit good repeatability on both peak load, mean force, CFE, absorbed energy or SEA. The sandwich tube [2GFRP-[0_4]-2GFRP]-#1 has an SEA slightly lower than tubes # 2 and # 3 because of a drop in the force of the plateau from 7000 N to 6000 N after about 30 mm of crushing (Fig. 14 (c)). This observation is the same for the sandwich tubes [2GFRP-[0_5]-2GFRP]-#1 (Fig. 14 (d)) and [2GFRP-[0_6]-2GFRP]-#1 and #2 (Fig. 14 (e)). This decrease in performance can be explained by a different failure mode. In fact, on the tube [2GFRP-[0_4]-2GFRP]-#1, a longitudinal, intralaminar crack appears at the start of crushing (at 27.9 mm) (Fig. 15 (a)). This large crack weakens the tube, then a second longitudinal, intralaminar crack appears around 38.3 mm and weakens the tube again. These cracks cause a drop in the force, which is then no longer distributed uniformly over the cross-section of the tube. On the other hand, a glance at the post-mortem patterns shows that the tube has lost all of its structural integrity, as evidenced by the presence of large

debris (Fig. 15 (a)). A smaller drop in plateau force is also observed for sandwich tube [2GFRP-[0_4]-2GFRP]-#3 around 40 mm of crushing. It is again due to longitudinal cracks, but they are smaller and do not cross the entire thickness of the tube, which reduces the impact on the dissipated energy.

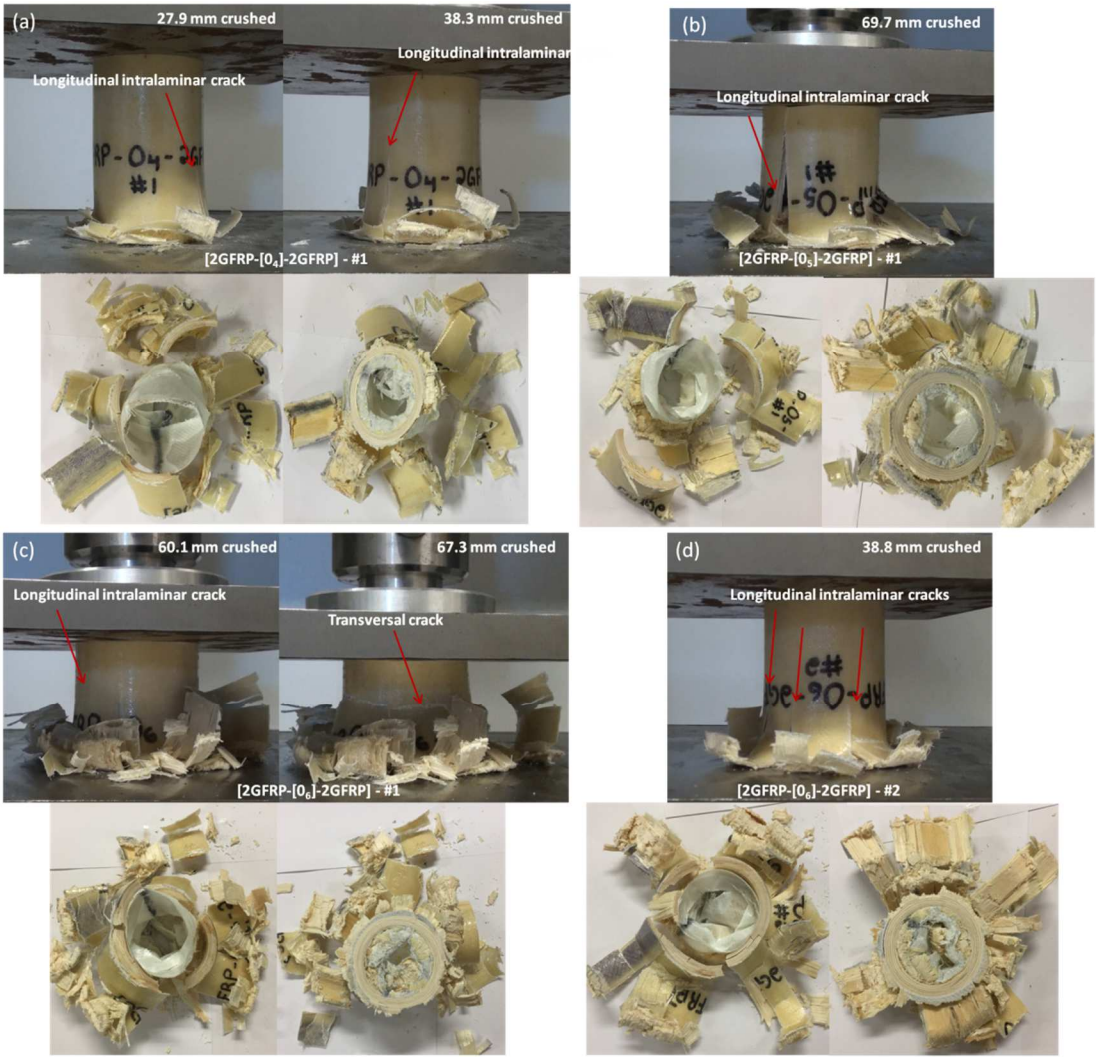

Fig. 15. Failure of tubes (a) [2GFRP-[0_4]-2GFRP]-#1, (b) [2GFRP-[0_5]-2GFRP]-#1, (c) [2GFRP-[0_6]-2GFRP]-#1, (d) [2GFRP-[0_6]-2GFRP]-#2 during crushing and post-mortem patterns.

The same observation can be made for the tube [2GFRP-[0_5]-2GFRP]-#1, with the appearance of a longitudinal, intralaminar crack around 49.3 mm long, which divides the tube right through its thickness (Fig. 15 (b)). Again, only a portion of the tube is able to withstand the stress and therefore does not provide an optimal response. Other longitudinal cracks appear as the crash progresses, further explaining the drop in stress at the end of the crash.

On the sandwich tube [2GFRP-[0_6]-2GFRP]-#1 (Fig. 15 (c)), a longitudinal crack again weakens the tube in the middle of the crushing (around 55 mm). Then, this crack propagates until another crack appears transverse to the axis of the tube, further weakening the structure. On the sandwich tube [2GFRP-[0_6]-2GFRP]-#2 (Fig. 15 (d)), three longitudinal cracks weaken the tube.

The initiation of failure occurs with the breaking of the glass fibres oriented at 90° on the outer skin under too large a strain. This 90° fibre break dissociates the tube into bundles, which then bend and splay. The predominant failure on these sandwich tubes is splaying. However, the failure patterns also show a debonding of the inner skins (Fig. 16), local buckling, and some tubes collapsing by fragmentation following significant longitudinal cracks. Sometimes, a certain portion of the thickness bends entirely without dissociating into two bundles. A difference in the behaviour of the inner and outer skins is to be noted. The outer skins undergo 90° fibre breaks and splay while the inner skins experience a debonding with the core and local buckling.

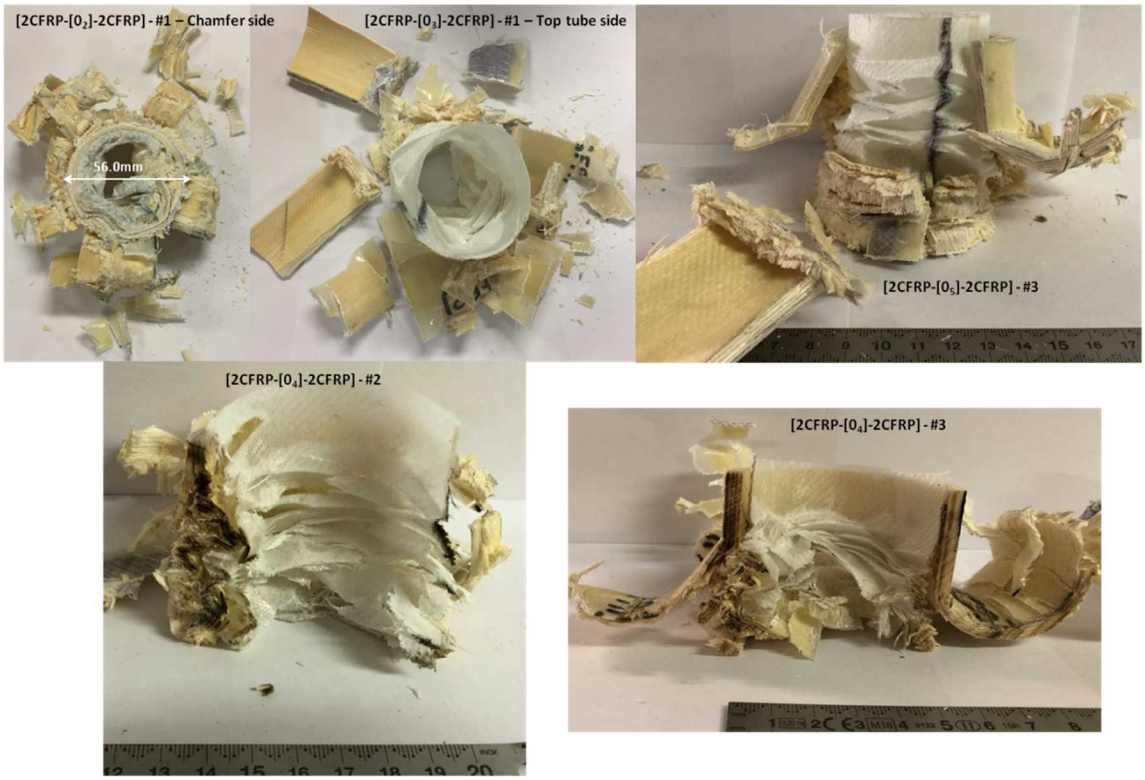

Fig. 16. Post-mortem patterns of tubes [2GFRP-[0_2]-2GFRP]-#1, [2GFRP-[0_3]-2GFRP]-#1 and [2GFRP-[0_5]-2GFRP]-#3 and the ½ tubes [2GFRP-[0_4]-2CFRP]-#2, [2GFRP-[0_4]-2GFRP]-#3

As with the carbon sandwich tubes, absorbed energy and SEA were plotted versus the number of layers of I214 (Fig. 17 (a)). The energy absorbed evolves linearly with the number of layers of I214: the

contribution of a ply of poplar here would be 430 J while the contribution of the fibreglass skins would be very slightly negative (-43 J). On the tubes with two and three I214 layers, the SEA is slightly lower than for tubes with 4, 5 or 6 plies. The maximum SEA is obtained for 6 layers with 42.8 J/g. The dispersion of the results increases again with the number of I214 layers.

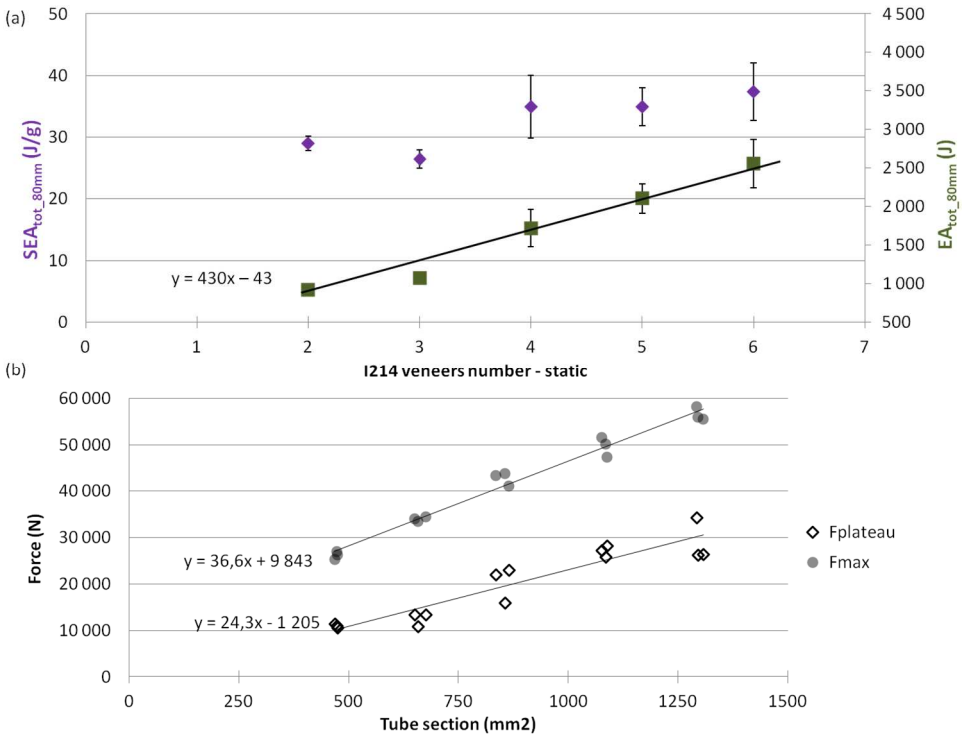

Fig. 17. (a) Evolution of l'EA_{tot_80mm} and SEA_{tot_80mm} versus the number of I214 layers, (b) Evolution of the peak force and the average plateau force versus the section of the tubes with glass fibre skins

As with carbon fibre skins, the average crushing stress of an I214 ply was calculated from linear regressions on the curves of stress as a function of the tube section (Fig. 17 (b)). The peak load curve gives a value of 36.6 MPa, very close to the values obtained for tubes with carbon skins. On the other hand, it is clearly lower in the plateau phase, with 24.3 MPa.

Once again, the y-intercept of the regression line associated with the peak load (9,843 N) shows that the glass fibre skins work better than in the plateau phase (- 1,205 N), but still not as well as the skins of wood/carbon sandwiches.

3.4. Skin/core coupling effect in sandwiches

The objective here was to observe the coupling effect between the poplar and the skins of carbon and glass fibres, i.e. to compare the levels of dissipated energy and the behaviour of the different materials

depending on whether they are crushed in a wood-only or composite-only configuration, or in a sandwich configuration. This study was performed for both CFRP and GFRP skins.

3.4.1. Carbon skins

This coupling study was first carried out on the [2CFRP-[90/0_4/90]-2CFRP] configuration. The [CFRP]-only tubes shown in Fig. 18 and Tab. 6, made of 4 woven carbon layers, were identical in diameter to the sandwich tube. Thus corresponding to the equivalent of the inner and outer skins of sandwich tubes [2CFRP-[90/0_4/90]-2CFRP]. Poplar tubes alone, corresponding to the core configuration [90/0_4/90] have already been crushed before in [26] (not recalled here), and also have the same diameter.

First, Fig. 18 shows the curves of the three crushes of 4-ply [CFRP] tubes. The three classic phases of a crush can be observed once again. The performances (Tab. 6) show an interesting average SEA of 66.7 J/g with one tube (# 3) presenting a slightly higher energy absorption than the other two. The failure mode is characterized by the gradual formation of petals via splaying (Fig. 19). The crush front shows splaying accompanied by failures in the laminate, which is almost the same as the front obtained by Guillon [27], defined as fragmented splaying.

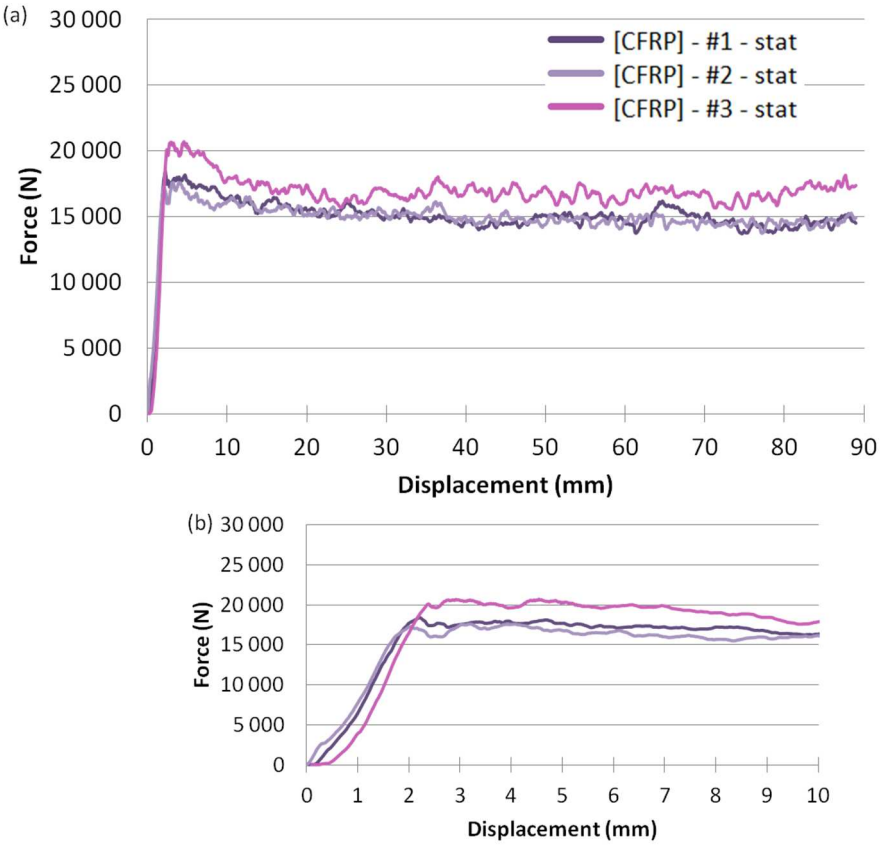

350

351 **Fig. 18. (a) Static crushing of carbon tubes (b) Zoom on initiation**

	Mass	Thickness	F_{max}	$L_{plateau}$	$F_{plateau}$	CFE	EA_{tot_80mm}	SEA_{tot_80mm}
	g	mm	N	mm	N		J	J/g
CFRP - #1	27.7	0.97	18 434	79.2	14 942	0.81	1 203	64.6
CFRP - #2	27.9	0.97	17 603	80.7	14 947	0.85	1 196	63.7
CFRP - #3	27.6	0.97	20 729	79.3	16 821	0.81	1 340	71.8
Average	**27.7**	**0.97**	**18 922**	**79.7**	**15 570**	**0.82**	**1 247**	**66.7**
Standard deviation	**0.2**	**0.00**	**1 619**	**0.8**	**1 083**	**0.02**	**81**	**4.5**

352 **Tab. 6. Static results for [CFRP] tubes.**

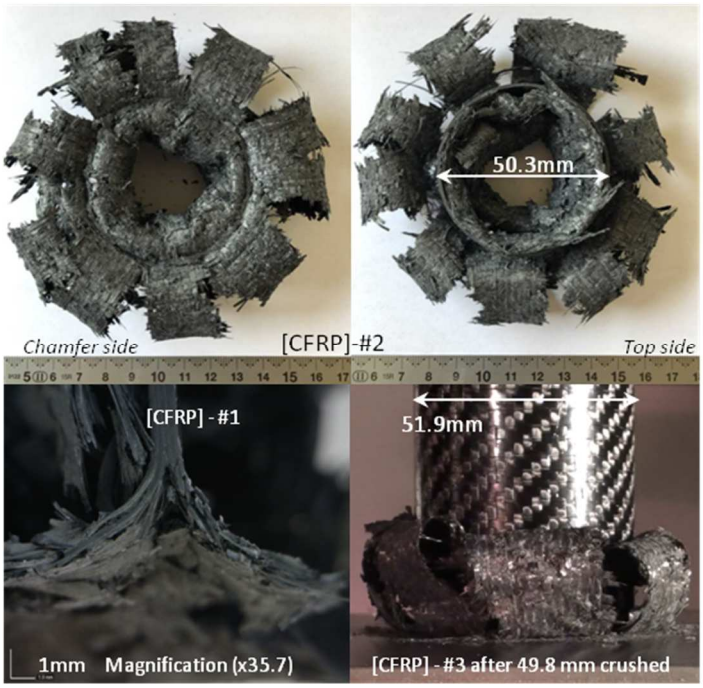

Fig. 19. Post-mortem patterns of tubes [CFRP] under static crushing.

By adding the crushing force/displacement curves of the tubes [CFRP] presented above and poplar tubes alone, we can compare the effect of materials alone and coupled materials (sandwich) (Fig. 20). The hatched part corresponds to the gain obtained by the association of carbon with wood in the sandwich. This gain has been quantified in Tab. 7, considering the sum of the plateau forces of the configurations [90/0_4/90] and [CFRP] and the equivalent SEA. The coupling of the carbon layers to the I214 poplar veneers thus allows a gain of 12% on the SEA compared to the behaviour observed in independent materials. However, the carbon tubes alone remain more efficient than the sandwich. In this configuration, the carbon fibres improve the performance of the I214 veneers relative to the wooden tubes alone, presumably by increasing the containment by the hoop effect, but the performance of the carbon skins is diminished, being in splaying-only mode.

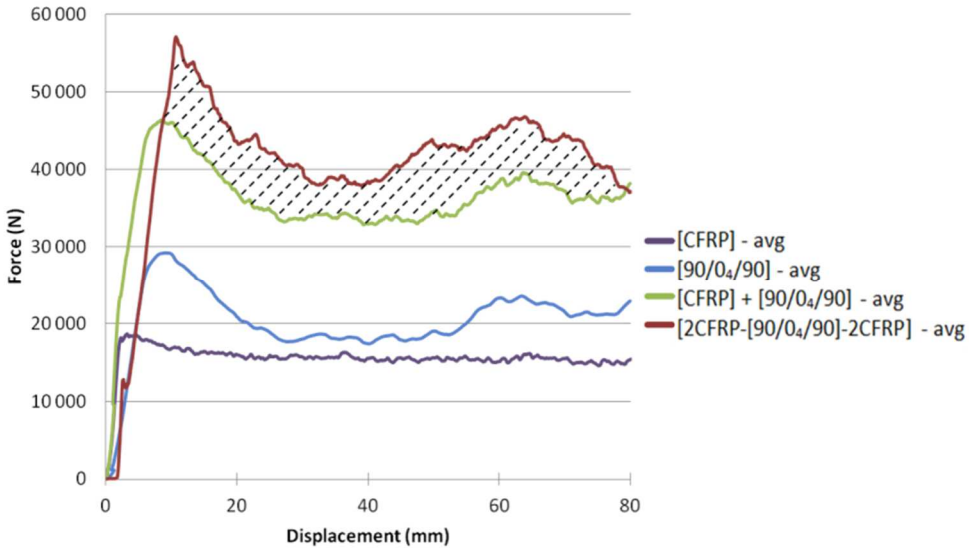

Fig. 20. Static coupling for sandwich [2CFRP-[90/0$_4$/90]-2CFRP].

	N $F_{plateau}$	J EA_{tot_80mm}	g Mass	J/g SEA_{tot_80mm}
[90/0$_4$/90] - avg	21 019	1 632	76.6	31.5
[CFRP] - avg	15 570	1 247	27.7	66.7
[90/0$_4$/90] + [CFRP] - avg	36 589	2 879	104.3	40.2
[2CFRP-[90/0$_4$/90]-2CFRP] - avg	41 328	3 248	103.22	45
Coupling effect	13%	13%		12%

Tab. 7. Gain obtained by coupling the two materials (carbon and poplar) on a sandwich [2CFRP-[90/0$_4$/90]-2CFRP]

This work is now carried out on the configuration [2CFRP- [0$_6$] -2CFRP] but, to evaluate the coupling effect, we do not consider the [0$_6$] core but the [90/0$_4$/90] core again. In fact, the crushing of poplar tubes with a stack [0$_6$] was studied in [26] and showed unstable crushing of the tubes with absence of a plateau and very low energy absorption, which would not allow a consistent coupling study to be carried out. Thus it was decided to make the comparison with the core [90/0$_4$/90], which gave the best results of the test campaign on wooden tubes alone, even though the contribution of the coupling for the configuration [2CFRP- [0$_6$] -2CFRP] is then underestimated.

As in the previous case, the crushing force/displacement curves of the tubes [CFRP] and poplar tubes with the core alone [90/0$_4$/90] are added together and the result compared with the curve of the configuration [2CFRP- [0$_6$] -2CFRP] (Fig. 21).

Tab. 8 shows the gain provided by the coupling effect in this configuration. Thus, combining carbon and wood allows a 52% gain in plateau force, energy absorbed is increased by 48%, and SEA by 47%. As in the previous configuration, the carbon fibre tubes alone remain more efficient in terms of SEA than the equivalent sandwich make-up, but by only 10%.

Thanks to the study of the influence of the number of poplar layers on the forces and energies presented in section 3.2, it is possible to quantify the gains or losses for each of the materials. The energy absorbed during the first 80 millimetres of crushing is linearly proportional to the number of folds, as is the plateau force (Tab. 4 and Fig. 13). Therefore the energy absorbed can be calculated on average by 1 ply of wood (575.6 J), and by the core (6 plies): 3,454 J. The energy dissipated in the skins for this sandwich is 4,264 – 3,454 = 810 J. These figures show that the wooden plies at 0° in the sandwich absorb more than twice as much energy as a wooden tube alone [90/0_4/90] (3,454 J against 1,632 J). In return, the skins absorb a little less (810 J against 1,247 J) and show that CFRP as skins in sandwich tubes works less efficiently than alone but stabilize well I214 poplar fibres oriented at 0° and enhanced wood fibres behaviour. This quantitative analysis shows that the hoop effect induced by the carbon fibres has a positive influence on the behaviour of poplar during crushing, via a change in failure mode (here mainly in flaring). This allows a significant increase in the energy absorbed in the tube, even if the failure mode in the skins does not allow an SEA as large as in the case of [CFRP] tubes alone to be obtained.

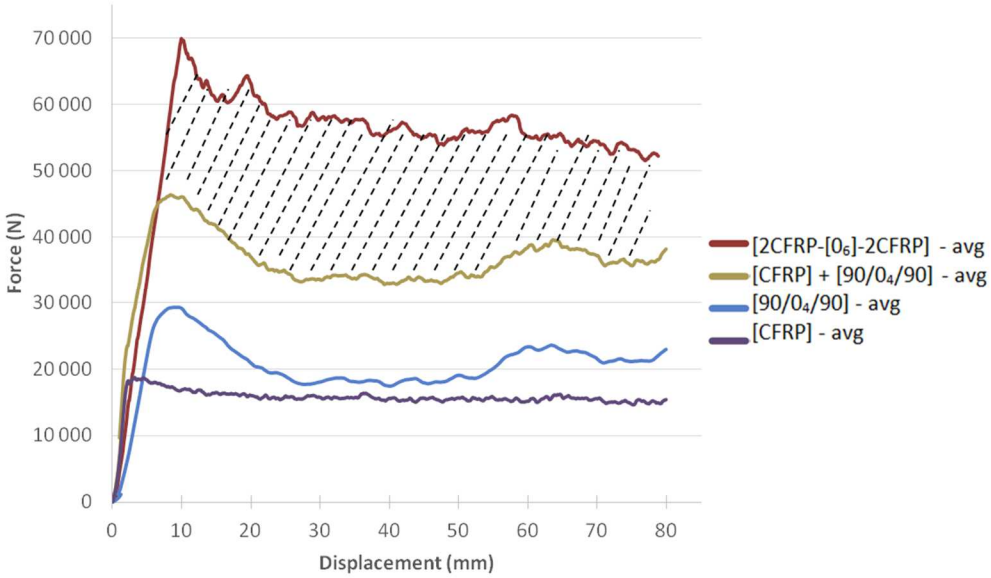

Fig. 21. Static coupling on sandwich [2CFRP-[0$_6$]-2CFRP].

	$F_{plateau}$ N	EA_{tot_80mm} J	Mass g	SEA_{tot_80mm} J/g
[90/0$_4$/90] – avg	21 019	1 632	76.6	30.6
[CFRP] – avg	15 570	1 247	27.7	66.7
[90/0$_4$/90] + [CFRP] – avg	36 589	2 879	104.3	40.6
[2CFRP-[0$_6$]-2CFRP] – avg	55 551	4 264	102.9	59.5
Coupling effect	52%	48%		47%

Tab. 8. Gain obtained by coupling the two materials (carbon and poplar) on a sandwich [2CFRP-[0$_6$]-2CFRP].

3.4.2. Glass skins

In the same way as with carbon skins, to evaluate the effect of skin/core coupling on sandwiches [GFRP], static compression tests were carried out on tubes made of 4 GFRP woven plies (Fig. 22). Once again, the three phases are found. The energy absorption performance is relatively low for these tubes (Tab. 9), as the level of effort on the plateau is low, generating a very small amount of energy (364 J) and an average SEA of 21.4 J/g. During the crush, fairly large pieces of debris can be observed. The dimensions are of the order of a few centimetres and they are larger in the circumferential direction than in the vertical one. They create a general instability of the walls of the tube, leading to little energy absorption (Fig. 23).

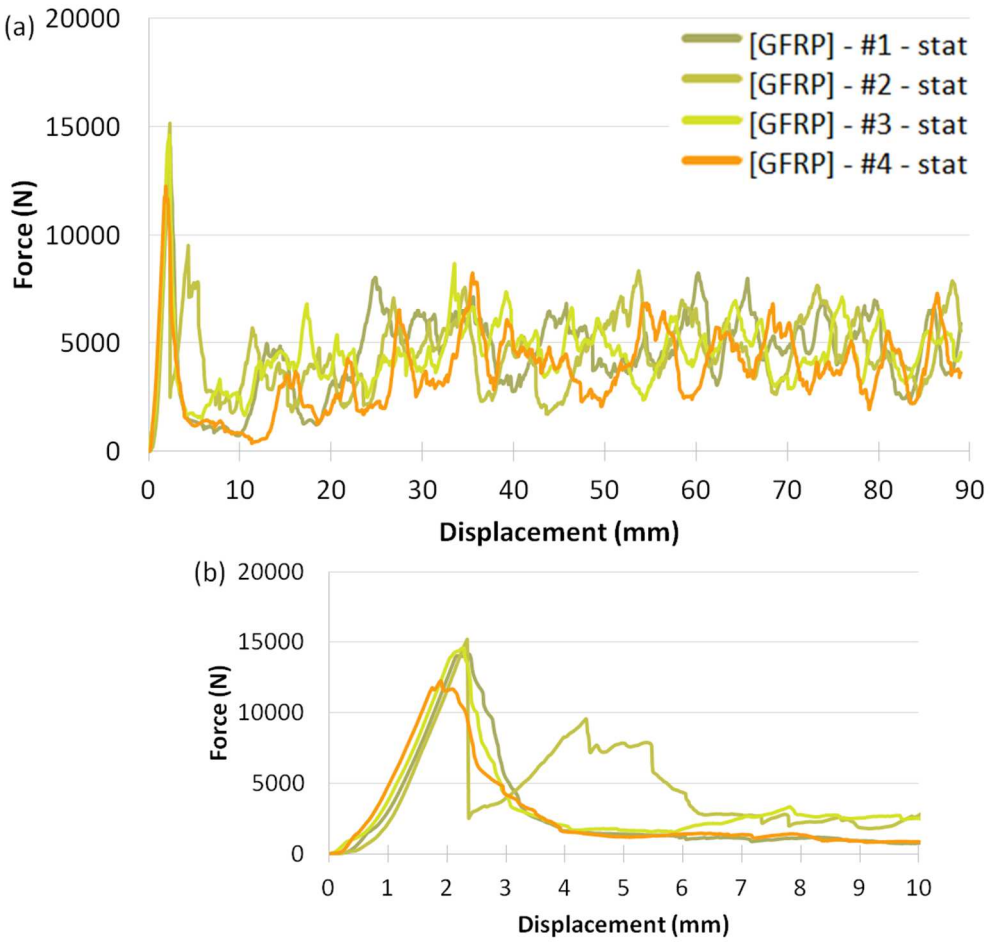

408
409 **Fig. 22. (a) Static crushing of glass tubes (b) Zoom on initiation**

	Mass g	Thickness mm	F_{max} N	$L_{plateau}$ mm	$F_{plateau}$ N	CFE /	EA_{tot_80mm} J	SEA_{tot_80mm} J/g
[GFRP] - #1	24.2	0.65	14 179	76.0	4 860	0.34	369	22.6
[GFRP] - #2	24.3	0.68	15 178	83.3	4 476	0.29	363	22.2
[GFRP] - #3	23.7	0.67	14 617	77.5	4 674	0.32	359	22.5
[GFRP] - #4	23.7	0.67	12 275	74.7	3 985	0.32	291	18.3
Average	**24.0**	**0.67**	**14 658**	**78.9**	**4 499**	**0.32**	**364**	**21.4**
Standard deviation	**0.3**	**0.01**	**1 260**	**3.8**	**377**	**0.02**	**37**	**2.1**

410 **Tab. 9. Results for static crushing of [GFRP] tubes**

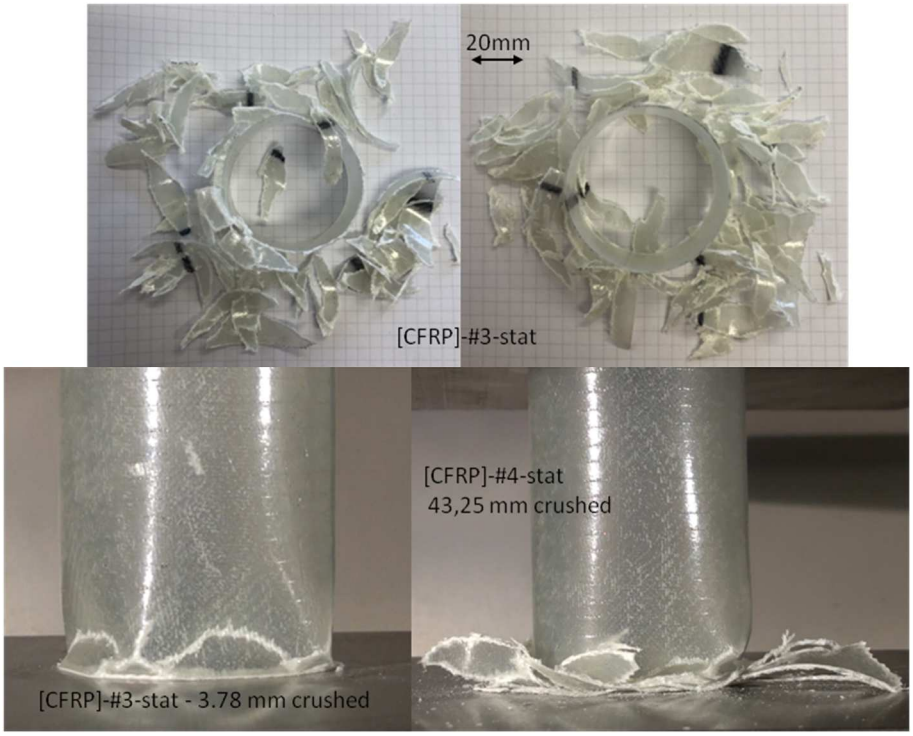

411

412 **Fig. 23. Failure patterns of [GFRP] tube (chamfer side: photo upper left; top of the tube: photo top right) – Detail at**
413 **initiation and for 43.25 mm of crushing (bottom photos)**

414 The combination of the [GFRP] skins and the core [90/0_4/90] then made it possible to obtain the
415 coupling provided by the sandwich (Fig. 24). The coupling in the sandwich increases greatly over ¾ of
416 the height measuring downwards from the crash and then undergoes a loss. This loss is due to the
417 tubes [2CFRP-[0_6]-2CFRP]-#1 and #2 which, at the end of the crash, experience a significant drop in
418 force. In total, a gain of 25% (Tab. 10) is obtained on the SEA between the crushing of the sandwich
419 tube and of a combination of the two tubes (skin and core) if they were crushed individually. For glass
420 fibre skins, the SEA of the sandwich tube is even greater than sum of the SEAs when each material is
421 taken separately. The difference with carbon fibre skins is that [GFRP] tubes alone dissipate very little
422 energy.

423

Fig. 24. Static coupling for a sandwich [2GFRP-[0$_6$]-2GFRP]

	$F_{plateau}$ N	EA_{tot_80mm} J	Mass g	SEA_{tot_80mm} J/g
[90/0$_4$/90] - avg	21 019	1 632	76.6	30.6
[GFRP] - avg	4 670	364	24.0	21.4
[90/0$_4$/90] + [GFRP] - avg	25 689	1 996	100.6	29.9
[2GFRP-[0$_6$]-2GFRP] - avg	28 995	2 556	99.24	37.4
Coupling effect	13%	28%		25%

Tab. 10. Gain obtained by a sandwich with GFRP skins and poplar core

3.5. Comparison of glass and carbon skins

Crushes of iso-cored sandwich tubes with glass and carbon skins allow comparisons to be made. The curves of the carbon fibre and glass fibre sandwich tubes are juxtaposed in Fig. 25.

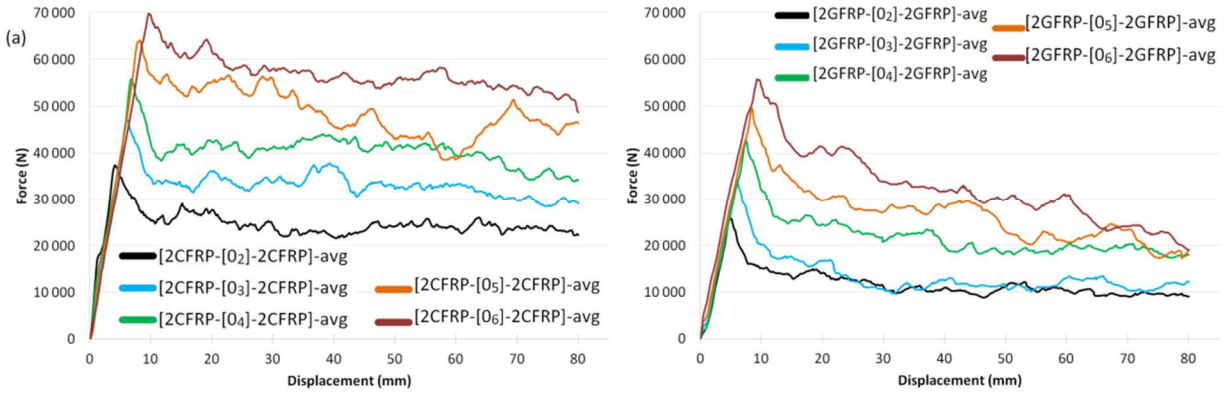

Fig. 25. Comparison of static crushing of sandwich tubes with CFRP skins (a) and GFRP skins (b)

The first observation concerns the levels of forces (peak and plateau) according to the number of poplar layers and skins. The fibreglass sandwich tubes are below the stress levels of the carbon fibre sandwich tubes for every configuration. The second observation concerns the slopes of the initial force increase,

435 calculated as stiffness: $\frac{\Delta F}{\Delta L}$ (Fig. 26 (b)). These slopes vary both with the nature of the fibre and with the
436 number of I214 layers. As the number of I214 plies increases, the apparent slope decreases for CFRP
437 skins but seems to be constant for GFRP skins. Fig. 26 (a) shows that the initial increase is, in fact, not
438 linear. During this phase of increasing force, the displacement is the sum of two phenomena: the local
439 crushing of the chamfer and the elastic response of all the rest of the pristine tube. The observed slope
440 variations (slopes 1 to 3 on Fig. 26 (a)) are mainly related to damage to the chamfer. Slope 1
441 corresponds to the crushing of the interior composite skin. When the wood begins to crush, a lower
442 slope (slope 2) starts, the crushing stress of the poplar being lower than that of the composite skins.
443 Finally, when the outer composite skin reaches the crushing plateau, the slope is found to be the same
444 as at the beginning (slope 3). In addition, it is observed that the stiffness of the carbon fibre sandwich
445 tubes is greater than that of the glass fibre sandwich tubes (Fig. 26 (b)), which is consistent with both
446 the lower compression strength of glass compared to carbon, and its lower stiffness.

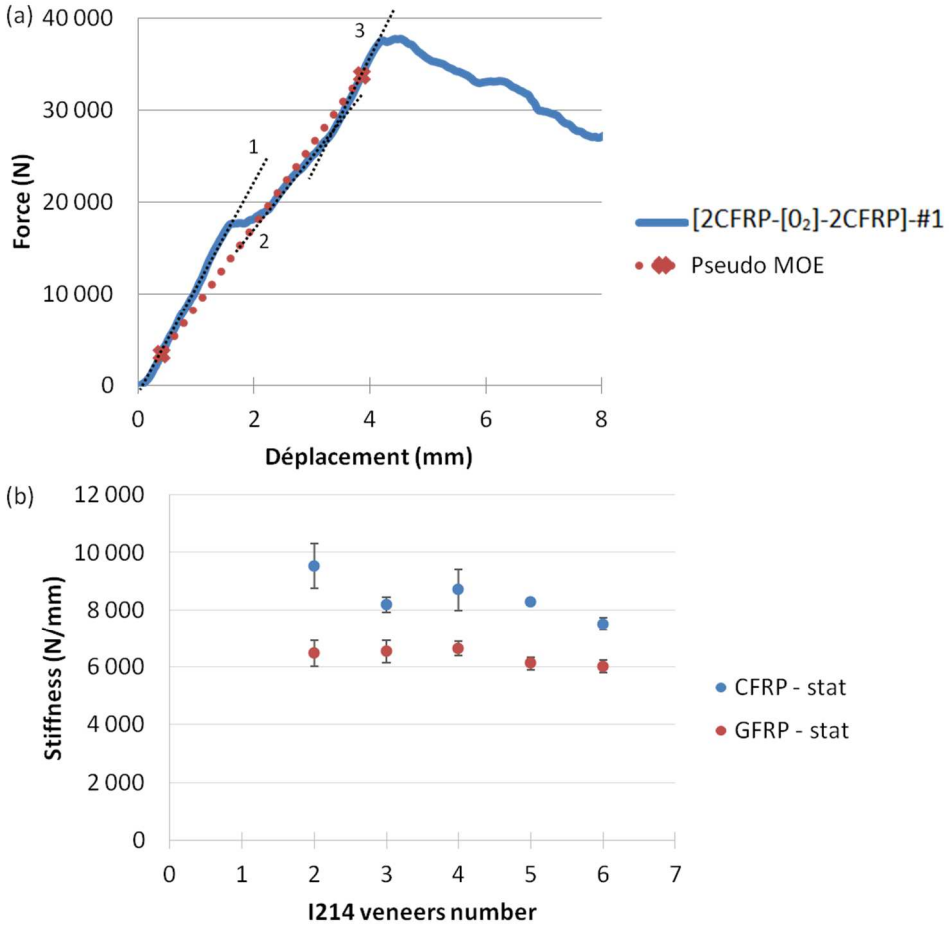

Fig. 26. Focus on initiation on CFRP sandwiches

Now let us consider the plateau phase. Globally, the modes of failure of the carbon and glass layers in the sandwich are similar, mainly with splaying due to failure in the fibres at 90°, which dissociate the tube into bundles that bend under the force and splay. The presence of local core buckling is observed in both types of sandwiches, and local buckling is also present on the inner fibreglass skins. It can also be seen on both types of sandwich tubes that part of the thickness bends entirely without splaying. However, on the glass sandwich tubes, significant debonding of the inner skins can be observed, the origin of which has not been identified. On the other hand, qualitatively, when crushed, fibreglass sandwich tubes exhibit much larger cracks in the direction of the tube axis than carbon fibre sandwich tubes do. These cracks weaken the structure of the tube and thus its response to crushing. These points, together with the lower crush resistance generally observed with glass compared to carbon, explain why glass sandwiches absorb much less energy than carbon sandwiches (Fig. 27). In addition,

460 to within a few grams, the carbon and glass sandwich tubes have the same mass (same basis weight
461 for the two prepregs), hence the same trend for SEA.
462 Finally, sandwich tubes with carbon fibre skins show a slight decrease in SEA (61.2 J/g on average)
463 relative to the SEA of carbon fibre tubes alone (66.7 J/g). Those made of glass show an increase in
464 SEA (32.5 J/g for 21.4 J/g with glass fibre tubes). The poplar core improves the behaviour of the glass
465 layer by stabilizing it, despite local debonding of the interior layers.

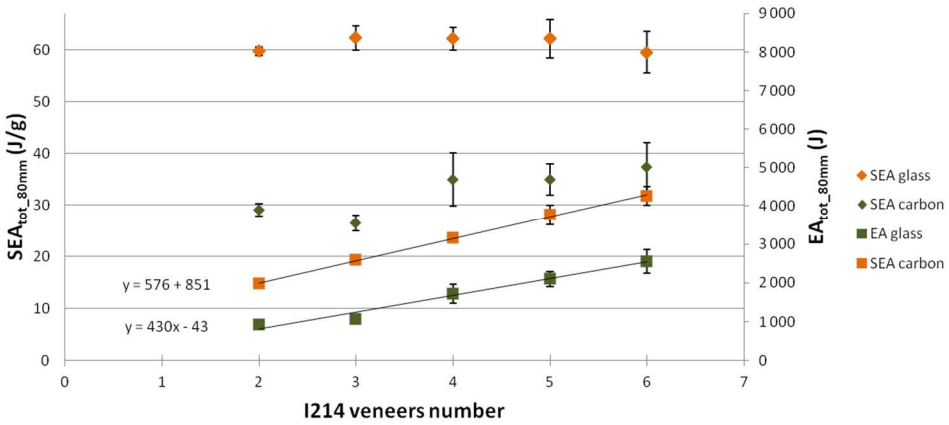

466
467 **Fig. 27. Evolution of EA$_{tot_80mm}$ and SEA$_{tot_80mm}$ with the number of I214 veneers and the nature of the skins**

468 ## 4. Conclusions and perspectives

469 The experimental static crushing of sandwich tubes having skins made with carbon or glass-epoxy resin
470 fibres has been studied here and the test results show that:

471 - For the core, it is preferable to orient all the poplar veneers at 0° for optimal energy absorption:
472 the "hoop effect" ensured by the outer and inner composite layers is sufficient.
473 - The crushing of tubes [2CFRP-[0_N]-2CFRP]$_{2\leq N\leq 6}$ has shown interesting energy absorption
474 results, with an average SEA of 61.2 J/g. The energy absorbed varies linearly with the number
475 of I214 plies used and the SEA is constant. Coupling poplar to carbon fibres gives rise to an
476 SEA gain of around 47% with respect to the sum of the two materials crushed independently.
477 The use of wood on such a sandwich structure (6 ply I214) also gives an SEA (59.5 J/g) that is
478 almost the same as that of the equivalent CFRP tube (66.7 J/g), with a higher level of energy
479 absorption (elevation of the crushing plateau: 55,551 N for sandwiches, 15,570 N for CFRP
480 tubes). The predominant mode of ruin is splaying. Local buckling is also observable.

- The crushing of tubes [2GFRP-[0_N]-2GFRP]$_{2\leq N\leq 6}$ also provides interesting energy absorption results. An average SEA of 32.5 J/g is obtained. The characteristic failure pattern of these tubes shows the formation of petals induced by splaying. On the other hand, a fairly significant debonding of the inner skins was observed. Coupling I214 poplar veneers with glass fibres allows, in particular, a gain of 20% on absorbed energy and 22% on the SEA. With the fibreglass skins, the insertion of the I214 veneers as the core material results in a higher SEA and a crushing plateau elevation due to the sandwich tube having 6 I214 plies (37.4 J / g , 28,995 N) compared to tube [GFRP] (21.4 J / g; 4,670 N).

Whether as a "layered" material [26], or as a core material, I214 poplar has demonstrated its capacity to contribute to crashworthiness. This static study shows interesting energy absorption results for both carbon and glass fibre skins, and dynamic crushes are now needed to better understand their dynamic behaviour. The crushing scenario between the wood veneers and the adhesive is not well known and should deserve more investigations to determine if the wood veneers are broken with a cohesive or adhesive rupture. Another interesting step in these studies will be the design of a technological crash box that can be used on a vehicle.

5. Acknowledgements

The authors thank the French Government for providing financial support (MESRI) and the Garnica company for providing I214 veneers for this study.

6. References

[1] Bucci V, Corigliano P, Crupi V, Epasto G, Guglielmino E, Marinò A. Experimental investigation on Iroko wood used in shipbuilding. Proc Inst Mech Eng Part C J Mech Eng Sci 2017;231:128–39. https://doi.org/10.1177/0954406216674495.

[2] Zenkerts D. The handbook of sandwich construction. Engineering Materials Advisory Services Ltd. United Kingdom: 1997.

[3] Butler N. Computer modelling of wood-filled impact limiters. Nucl Eng Des 1994;150:417–24. https://doi.org/10.1016/0029-5493(94)90161-9.

[4] Forest Products Laboratory. Wood Handbook—Wood as an Engineering Material. United States Department of Agriculture Forest Service; 2010.

[5] Bergman R, Puettmann M, Taylor A, Skog KE. The Carbon Impacts of Wood Products. For Prod J 2014;64:220–31. https://doi.org/10.13073/FPJ-D-14-00047.

[6] Castanie B, Bouvet C, Ginot M. Review of composite sandwich structure in aeronautic applications. Compos Part C Open Access 2020;1:100004. https://doi.org/10.1016/j.jcomc.2020.100004.

[7] Magee C, Page J. 2019. https://drive-my.com/en/test-drive/item/3893-1966-costin-nathan.html.

[8] Asada R, Cardellini G, Mair-Bauernfeind C, Wenger J, Haas V, Holzer D, Stern T. Effective bioeconomy? a MRIO-based socioeconomic and environmental impact assessment of generic sectoral innovations. Technol Forecast Soc Change 2020;153:119946. https://doi.org/10.1016/j.techfore.2020.119946.

[9] Kohl D, Link P, Böhm S. Wood as a Technical Material for Structural Vehicle Components. Procedia CIRP 2016;40:557–61. https://doi.org/10.1016/j.procir.2016.01.133.

[10] Müller U, Jost T, Kurzböck C, Stadlmann A, Wagner W, Kirschbichler S, et al. Crash simulation of wood and composite wood for future automotive engineering. Wood Mater Sci Eng 2020;15:312–24. https://doi.org/10.1080/17480272.2019.1665581.

[11] Consortium WoodC.A.R. n.d. https://www.woodcar.eu/index.html.

[12] Susainathan J, Eyma F, De Luycker E, Cantarel A, Castanie B. Manufacturing and quasi-static bending behavior of wood-based sandwich structures. Compos Struct 2017;182:487–504. https://doi.org/10.1016/j.compstruct.2017.09.034.

[13] Smardzewski J, Wojciechowski KW. Response of wood-based sandwich beams with three-dimensional lattice core. Compos Struct 2019;216:340–9. https://doi.org/10.1016/j.compstruct.2019.03.009.

[14] Kavermann SW, Bhattacharyya D. Experimental investigation of the static behaviour of a corrugated plywood sandwich core. Compos Struct 2019;207:836–44. https://doi.org/10.1016/j.compstruct.2018.09.094.

[15] Smardzewski J. Experimental and numerical analysis of wooden sandwich panels with an auxetic core and oval cells. Mater Des 2019;183:108159. https://doi.org/10.1016/j.matdes.2019.108159.

[16] Wang X, Shi X, Meng Q, Hu Y, Wang L. Bending behaviors of three grid sandwich structures with wood facing and jute fabrics/epoxy composites cores. Compos Struct 2020;252:112666. https://doi.org/10.1016/j.compstruct.2020.112666.

[17] EASA. European Aviation Safety Agency, Certification Specifications for Large Aeroplanes - CS25, Admendment 2009.

[18] Atas C, Sevim C. On the impact response of sandwich composites with cores of balsa wood and PVC foam. Compos Struct 2010;93:40–8. https://doi.org/10.1016/j.compstruct.2010.06.018.

[19] Susainathan J, Eyma F, De Luycker E, Cantarel A, Castanie B. Experimental investigation of impact behavior of wood-based sandwich structures. Compos Part Appl Sci Manuf 2018;109:10–9. https://doi.org/10.1016/j.compositesa.2018.02.029.

[20] Demircioğlu TK, Balıkoğlu F, İnal O, Arslan N, Ay I, Ataş A. Experimental investigation on low-velocity impact response of wood skinned sandwich composites with different core configurations. Mater Today Commun 2018;17:31–9. https://doi.org/10.1016/j.mtcomm.2018.08.003.

[21] Susainathan J, Eyma F, De Luycker E, Cantarel A, Bouvet C, Castanie B. Experimental investigation of compression and compression after impact of wood-based sandwich structures. Compos Struct 2019;220:236–49. https://doi.org/10.1016/j.compstruct.2019.03.095.

[22] Susainathan J, Eyma F, DE Luycker E, Cantarel A, Castanie B. Numerical modeling of impact on wood-based sandwich structures. Mech Adv Mater Struct 2020;27:1583–98. https://doi.org/10.1080/15376494.2018.1519619.

[23] Balıkoğlu F, Demircioğlu TK, İnal O, Arslan N, Ataş A. Compression after low velocity impact tests of marine sandwich composites: Effect of intermediate wooden layers. Compos Struct 2018;183:636–42. https://doi.org/10.1016/j.compstruct.2017.08.003.

[24] Fatima NS, Dhaliwal GS, Newaz G. Influence of interfacial adhesive on impact and post-impact behaviors of CFRP/end-grain balsawood sandwich composites. Compos Part B Eng 2021;212:108718. https://doi.org/10.1016/j.compositesb.2021.108718.

[25] Adalian C, Morlier P. "WOOD MODEL" for the dynamic behaviour of wood in multiaxial compression. Holz Als Roh- Werkst 2002;60:433–9. https://doi.org/10.1007/s00107-002-0333-x.

[26] Guélou R, Eyma F, Cantarel A, Rivallant S, Castanié B. Crashworthiness of poplar wood veneer tubes. Int J Impact Eng 2020:103738. https://doi.org/10.1016/j.ijimpeng.2020.103738.

[27] Guillon D. Etude des mécanismes d'absorption d'énergie lors de l'écrasement progressif de structures composites à base de fibre de carbone. PhD Thesis. Institut Supérieur de l'Aéronautique et de l'Espace, ISAE, Ecole doctorale : Mécanique, énergétique, génie civil et procédés, 2008.

[28] Farley GL. Energy absorption of composite materials. J Compos Mater 1983;17:267–79. https://doi.org/10.1177/002199838301700307.

[29] Hull D. A unified approach to progressive crushing of fibre-reinforced composite tubes. Compos Sci Technol 1991;40:377–421. https://doi.org/10.1016/0266-3538(91)90031-j.

[30] Chambe J, Bouvet C, Dorival O, Ferrero J. Energy absorption capacity of composite thin-wall circular tubes under axial crushing with different trigger initiations. J Compos Mater 2019:002199831987722. https://doi.org/10.1177/0021998319877221.

[31] Kindervater CM. Energy absorption of composites as an aspect of aircraft structural crash-resistance. Dev. Sci. Technol. Compos. Mater., Springer Netherlands; 1990, p. 643–51. https://doi.org/10.1007/978-94-009-0787-4_89.

[32] Thornton PH, Edwards PJ. Energy absorption in composite tubes. J Compos Mater 1982;16:521–45. https://doi.org/10.1177/002199838201600606.

[33] F Neveu, B Castanié, P Olivier. The GAP methodology: a new way to design composite structures, Materials & Design 2019, 172, 107755 https://doi.org/10.1016/j.matdes.2019.107755

[34] Tarlochan F, Ramesh S, Harpreet S. Advanced composite sandwich structure design for energy absorption applications: Blast protection and crashworthiness. Compos Part B Eng 2012;43:2198–208. https://doi.org/10.1016/j.compositesb.2012.02.025.

[35] Yan L, Chouw N, Jayaraman K. Effect of triggering and polyurethane foam-filler on axial crushing of natural flax/epoxy composite tubes. Mater Des 1980-2015 2014;56:528–41. https://doi.org/10.1016/j.matdes.2013.11.068.

[36] Zarei HR, Kröger M. Optimization of the foam-filled aluminum tubes for crush box application. Thin-Walled Struct 2008;46:214–21. https://doi.org/10.1016/j.tws.2007.07.016.

[37] Sun G, Wang Z, Hong J, Song K, Li Q. Experimental investigation of the quasi-static axial crushing behavior of filament-wound CFRP and aluminum/CFRP hybrid tubes. Compos Struct 2018;194:208–25. https://doi.org/10.1016/j.compstruct.2018.02.005.

[38] Sun G, Li S, Liu Q, Li G, Li Q. Experimental study on crashworthiness of empty/aluminum foam/honeycomb-filled CFRP tubes. Compos Struct 2016;152:969–93. https://doi.org/10.1016/j.compstruct.2016.06.019.

[39] Liu Q, Mo Z, Wu Y, Ma J, Tsui GCP, Hui D. Crush response of CFRP square tube filled with aluminum honeycomb. Compos Part B Eng 2016;98:406–14. https://doi.org/10.1016/j.compositesb.2016.05.048.

[40] Lindstrom A, Hallstrom S. Energy absorption of SMC/balsa sandwich panels with geometrical triggering features. Compos Struct 2010;92:2676–84. https://doi.org/10.1016/j.compstruct.2010.03.018.

[41] Stapleton SE, Adams DO. Crush Initiators for Increased Energy Absorption in Composite Sandwich Structures. J Sandw Struct Mater 2008;10:331–54. https://doi.org/10.1177/1099636208091737.

[42] Singace AA. Collapse behaviour of plastic tubes filled with wood sawdust. Thin-Walled Struct 2000;37:163–87. https://doi.org/10.1016/s0263-8231(00)00012-4.

[43] Kiran R, Khandelwal N, Tripathi P. Collapse behaviour and energy absorption of aluminium tubes filled with wood sawdust. Int J Eng Res Rev 2014.

[44] Reddy TY, Al-Hassani STS. Axial crushing of wood-filled square metal tubes. Int J Mech Sci 1993;35:231–46. https://doi.org/10.1016/0020-7403(93)90078-9.

[45] Siromani D, Henderson G, Mikita D, Mirarchi K, Park R, Smolko J, et al. An experimental study on the effect of failure trigger mechanisms on the energy absorption capability of CFRP tubes under axial compression. Compos Part Appl Sci Manuf 2014;64:25–35. https://doi.org/10.1016/j.compositesa.2014.04.019.

[46] Lavalette, Anne. 2014. « Développement de contreplaqués pour la construction navale : caractérisation multiéchelle et compréhension des phénomènes de collage du pin maritime à l'état vert ». Bordeaux: I2M - Institut de Mécanique et d'Ingénierie de Bordeaux.

[47] François, Patrice. 1992. « Plasticité du bois en compression multiaxiale : application à l'absorption d'énergie mécanique ». PhD Thesis, Université Bordeaux I. http://www.theses.fr/1992BOR10641.

[48] Blazy J-S. Comportement mécanique des mousses d'aluminium : caractérisations experimentales sous sollicitations complexes et simulations numériques dans le cadre de l'élasto-plasticité compressible. PhD Thesis. Ecole Nationale Supérieure des Mines de Paris, 2003.

[49] Israr HA, Rivallant S, Barrau JJ. Experimental investigation on mean crushing stress characterization of carbon–epoxy plies under compressive crushing mode. Compos Struct 2013;96:357–64. https://doi.org/10.1016/j.compstruct.2012.09.022.